SCIENTIFIC REPORTS
natureresearch

OPEN

The control of acidity in tumor cells: a biophysical model

Nicola Piasentin[1,3,4], Edoardo Milotti[1] & Roberto Chignola[2]✉

Acidosis of the tumor microenvironment leads to cancer invasion, progression and resistance to therapies. We present a biophysical model that describes how tumor cells regulate intracellular and extracellular acidity while they grow in a microenvironment characterized by increasing acidity and hypoxia. The model takes into account the dynamic interplay between glucose and O_2 consumption with lactate and CO_2 production and connects these processes to H^+ and HCO_3^- fluxes inside and outside cells. We have validated the model with independent experimental data and used it to investigate how and to which extent tumor cells can survive in adverse micro-environments characterized by acidity and hypoxia. The simulations show a dominance of the H^+ exchanges in well-oxygenated regions, and of HCO_3^- exchanges in the inner hypoxic regions where tumor cells are known to acquire malignant phenotypes. The model also includes the activity of the enzyme Carbonic Anhydrase 9 (CA9), a known marker of tumor aggressiveness, and the simulations demonstrate that CA9 acts as a nonlinear pH_i equalizer at any O_2 level in cells that grow in acidic extracellular environments.

Acid homeostasis in animal tissues is achieved by active dynamic processes. In physiological conditions, the pH of tissues is maintained between 7.35 and 7.45 in spite of constant metabolic acid production by cells. At the microscopic level, cells must finely regulate their own internal pH to around 7.2 to avoid death[1–3]. Cellular acid homeostasis is carried out by active transport of acid/base equivalents across the cell membranes into the extracellular spaces.

Dysregulation of pH is a well-known hallmark of solid tumors[1–3]. The tissue of solid tumors is characterized by the presence of an irregular network of blood vessels, causing a spatially heterogeneous delivery of nutrients such as glucose and oxygen to tumor cells[1–4]. As the consequence, the inner regions of solid cancers that are distant from blood vessels become hypoxic and acidic. Cancer cells adapt to such adverse environments through a series of molecular changes that involve an increased expression of nutrient and ion transporters and enzymes (reviewed in[1,3,5]). For example, hypoxia activates the Hypoxia Inducible Factor-1α (HIF-1α) that up-regulates the transcription of glucose transporters and of enzymes involved in glucose metabolism. Because of hypoxia, glucose is converted mainly to lactic acid through the glycolytic pathway to produce energy under the form of ATP, and the increased production of lactate reduces the pH of the extracellular spaces. A drop in intracellular pH, in turn, increases the activity of lactate and of various ion transporters that collectively contribute to recover intracellular acid homeostasis[1,3,5]. Hypoxia also causes the increased expression of some membrane-bound enzymes such as Carbonic Anhydrase (CA) that, on the cell surface, catalyzes the hydration of carbon dioxide (CO_2) to protons (H^+) and bicarbonate (HCO_3^-) ions. While the H^+ ions contribute to the acidity of the extracellular milieu, HCO_3^- ions can be transported back into the cells and increase the buffering potential of the intracellular environment[1,3,5], further contributing to maintain the intracellular pH at normal values.

It has recently been pointed out[1,3] that changes in the control of intracellular and extracellular acidity in the tissue of solid tumors are associated with many phenotypic changes of cancer cells with important implications in tumorigenesis, cancer progression, cancer diffusion, escape from immune surveillance and resistance to therapies. For example, microscopic examination of the tumor/normal tissue interface shows that peritumoral acidity drives tumor invasion in the surrounding normal tissue, with the regions of highest tumor invasion corresponding to those of lowest pH. In these regions the environmental pH reaches values that are toxic for normal but not for tumor cells[2].

[1]Department of Physics, University of Trieste, Via Valerio 2, 34127 Trieste, Italy. [2]Department of Biotechnology, University of Verona, Strada Le Grazie 15 - CV1, 37134 Verona, Italy. [3]Present address: Department of Chemical and Process Engineering, University of Surrey, Guildford GU2 7XH, UK. [4]Present address: Unilever Research Colworth, Colworth Park, Sharnbrook, Bedfordshire MK44 1LQ, UK. ✉email: roberto.chignola@univr.it

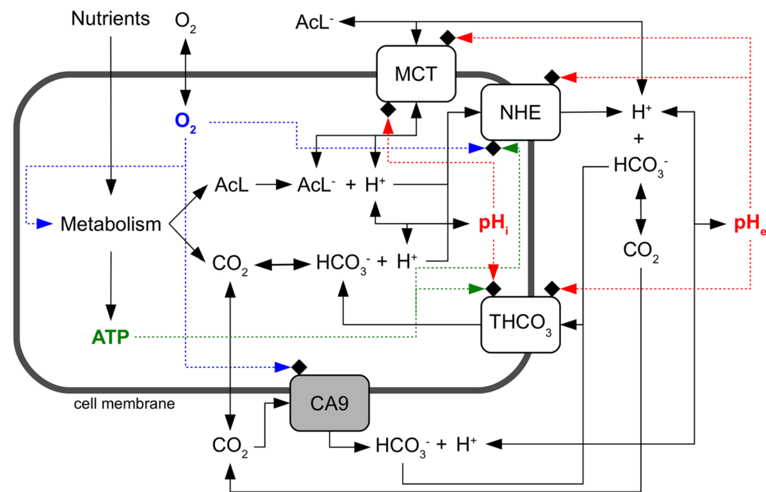

Figure 1. Layout of the model of acidity control in tumor cells. A cell takes up from the environment nutrients and oxygen which are then converted by cell metabolism to lactic acid, CO_2 and ATP. Lactic acid dissociates to lactate and H^+ ions, whereas CO_2 reversibly hydrates to HCO_3^- and H^+. These chemical species diffuse through cell membranes (CO_2) or are actively transported outside and eventually inside the cell by means of specific protein transporters. We consider monocarboxylate (MCT), sodium-hydrogen exchanger (NHE) and generic bicarbonate ($THCO_3$) transporters. We also model the activity of the membrane-bound enzyme Carbonic Anhydrase 9 (CA9). Chemical reactions are indicated by solid lines and the regulatory pathways by dashed lines. Proton concentrations inside and outside the cell are used to compute the intracellular (pH_i) and the extracellular (pH_e) pH. Detailed information on each pathway is given in the main text.

Biophysical models can help to disentangle the intricate relationships between regulatory biochemical networks and give support to the interpretation of experimental evidence which is rapidly accumulating in this field. In this paper we describe a comprehensive biophysical model of the control of acidity in tumor cells. We study the action of key molecular actors in acid homeostasis of cancer cells, and investigate to which extent hypoxia and environmental acidosis influence their behavior. We focus on the dynamic interplay between lactate, proton, bicarbonate transporters and CA enzyme, and their regulation by oxygen and both extracellular and intracellular pH. The model includes the bicarbonate buffer that acts both in the extracellular and intracellular milieus and it incorporates results from our previous modeling efforts concerning tumor cell metabolism[6–8]. In particular, our previous models provide values for the rates of glucose and oxygen uptake, lactate and CO_2 production and lactate/H^+ transport across cell membranes through specific transporters that have already been validated with experimental data. Finally, we fix the model parameters by combining information from a number of experiments carried out with different tumor cell systems.

Results

Preliminary considerations, model assumptions and parameters. We start from the rather detailed model of tumor cell metabolism and growth that we developed in our previous research[6–8] which successfully reproduces the observed behavior of tumor cells in both liquid (e.g. blood tumors) and solid tumors. In particular, for the current work we have excerpted from that model the part that describes the rates of glucose conversion to lactic acid and oxygen consumption. We remark that the model in[6–8] has been set up with the minimal set of chemical and biochemical pathways that drive the dynamics of metabolism and that are common to most, if not all, tumor cells.

Unlike the metabolic model in[6–8], here we must follow the dynamics of CO_2, HCO_3^- and H^+, both inside and outside a tumor cell. The inputs of the model are the rates of lactate and CO_2 production (Fig. 1) that depend on how cells take up nutrients, such as glucose, and convert them to ATP through the glycolytic and the oxidative phosphorylation pathways. Lactic acid dissociates immediately to lactate and H^+ ions, and both ions are transported through the cell membrane by means of the bi-directional monocarboxylate transporters MCT[6–8]. We remark that this part of the model impacts the rate of change of both intracellular and extracellular pH (from now on pH_i and pH_e, respectively), and oxygen is assumed to diffuse freely through the cell membrane and its consumption rate is used to determine the rate of CO_2 production.

Intracellular H^+ ions are transported outside the cell by means of unidirectional sodium-hydrogen exchangers NHE[1]. Different HCO_3^- transporters on the other hand are known to drive the flux of bicarbonate ions through the cell membrane. Some of them import or export HCO_3^- by exchanging Cl^- anions and the transport may depend or not on the presence of Na^+ cations[1]. Experimental works, however, have shown that the efficiency of HCO_3^- transport in different cell systems is quite similar, and that the import of HCO_3^- is fundamental in tumor cells where it is dominated by the activity of the Na^+-dependent Cl^-/HCO_3^- exchanger[9,10]. Therefore, we consider the import activity of a generic HCO_3^- transporter ($THCO_3$ in Fig. 1) which, as a first approximation, assumes the average biochemical characteristics of the Na^+-dependent Cl^-/HCO_3^- exchanger. We finally model the activity

of the membrane-bound Carbonic Anhydrase 9 (CA9) enzyme that catalyzes, on the cell surface, the hydration of CO_2. This is an important path since CA9 has been found to be expressed by many solid tumors of different histotypes, and its activity has been correlated to tumor progression and growth[11–13].

It should be noted in Fig. 1 that we do not take into account a possible effect of the extracellular pH on CA9 activity. Previous work has shown that CA9 in cell membrane extracts is sensitive to low pH and is completely inhibited at pH 6.0[14], its pH sensitivity being much steeper than that of other CA isoforms[15]. This observation, however, is at odd with findings obtained using high-resolution techniques with purified enzyme: they showed that the catalytic domain of human CA9, but not of other isoforms, is stable and active still at very low non-physiologic pH but inactive at pH > 8.0[16]. Because of these discrepancies, and since we do not want to focus on some specific cell system but rather to keep the model as general as possible, we decided to leave off the possible pH sensitivity of CA9 from the present model. Our modelling strategy is flexible enough to incorporate additional specific details when available, provided they are based on firm experimental conclusions.

We model the kinetics of ion transporters, and of CA9 activity as well, with the Michaelis-Menten/Hill formalism that is described by the following general equation:

$$\frac{d[X]_{C,c}}{dt} = \frac{V_{\max}[X]_{C,c}^h}{K_{\mathrm{m}}^h + [X]_{C,c}^h}$$

where $[X]_{C,c}$ is the molar concentration of a given chemical species inside ($[X]_C$) or outside ($[X]_c$) the cell, V_{max} and K_m are the Michaelis-Menten parameters and h is the Hill exponent ($h > 0$).

We assume that:

- CO_2 can freely diffuse through the cell membrane;
- CO_2 diffusion is driven by the concentration gradient across the membrane and its only important component is the one directed normally with respect to the cell membrane;
- the diffusion kinetics of charged ions through the cell membrane are much slower than the kinetics of the other processes in which they are involved, and thus the diffusion of charged ions is negligible;
- the mixing of all chemical species in the cell and in the external environment is instantaneous;
- within the short characteristic times of the considered chemical reactions the cell volume is constant.

In this work the variables take the following units for length, mass and time, respectively: μm, pg and s. Molar concentrations (M) have always been converted to mass units by taking into account the volume of the cell (V_C, cell volume is computed by approximating a cell to a sphere of given radius r_C) or of the environment (V_c) and the molecular mass (MW) of chemical species.

The model defined by the set of differential equations 11 has several parameters. We extensively searched the scientific literature to find their values, and when these values were not directly available they were obtained by fit of specific equations to reported experimental data. Experimental evidence was also used to model regulatory functions given by Eqs. 3, 5, 7 and 10 that tune the activity of transporters and CA9 enzyme as the function of local pH, ATP and/or oxygen availability. The full strategy is detailed in the Supplementary Material and all parameter values are listed in Table 1.

Once determined, parameter values were fixed and no further tuned to adapt model outputs to data. This means that the model has no free parameters and is strictly predictive. As explained in the next section, for validation purposes we first used it to predict how the intracellular pH (pH_i) varies when cells are grown into environments with increasing acidity.

Model validation with independent experimental data. Model validation was performed with independent experimental data, i.e. data that were not used to set parameter values. To this end we used the data in the paper by Song et al.[23]. In this paper Song et al. investigated the dependence of pH_i on pH_e in SCK cells (human choloangiocarcinoma cell line) in standard *in vitro* cultures. To the best of our knowledge no data concerning the direct expression of specific ion transporters and CA9 in these cells are available. However, the pH_i of SCK cells was measured in experiments where cells were also treated with Amiloride and DIDS inhibitors. Amiloride inhibits Na^+ channels and thus inhibits sodium-hydrogen exchangers, whereas DIDS inhibits all bicarbonate-dependent transport mechanisms (see Song et al.[23] and references cited therein). Thus, the expression of proton and bicarbonate transporters was functionally demonstrated in SCK cells. We do not know if SCK cells express CA9 but, as we shall see below (see Fig. 5), CA9 activity becomes negligible for pH_i regulation when the extracellular volume becomes higher than 10^4 cell volumes, i.e. when the extracellular volume exceeds $\sim 0.02\,\mu$l (the volume of 1 cell of radius $\sim 7\,\mu$m is ~ 2 pl). The experiments were carried out with cells kept under standard culture conditions where the extracellular volume is much higher, and thus it is irrelevant whether SCK cells express CA9 or not. Data obtained with SCK cells can therefore be used to validate the core model as far as the regulation of pH_i due to the activity of ion transporters is concerned.

The radius of SCK cells is not reported nor, to the best of our knowledge, it has been measured previously. This is important because our model equations take into account both cell volume (see Eqns. 1–11) and the cell surface (see e.g. CO_2 diffusion, Eq. 1) that are computed from cell radius under the assumption that cell geometry can be approximated by a sphere. Thus we run simulations for different cell radii whose values were taken within a reasonable range for animal cells.

Figure 2 shows the model prediction for intracellular pH vs. cell size, under standard culture conditions. At equilibrium there is a difference of ≈ 0.1 in pH between small and large cells ($r_C = 5.5$ and $8.0\,\mu$m, respectively, i.e. a volume ratio of $\simeq 3$) but pH_i levels reach values that have actually been observed in tumor cells[23]. With the

Parameter	Value	Unit	Reference
MW_H	1	$g\ mol^{-1}$	–
MW_{CO_2}	44	$g\ mol^{-1}$	–
MW_{O_2}	32	$g\ mol^{-1}$	–
MW_{HCO_3}	61	$g\ mol^{-1}$	–
MW^a_{AcL}	90.1	$g\ mol^{-1}$	–
P^b_{M,CO_2}	3.2×10^4	$\mu m\ s^{-1}$	[17]
gAcL	3.8×10^{-4}	$pg\ s^{-1}$	[6]
qO_2	3.5×10^{-5}	$pg\ s^{-1}$	[6]
k_1	0.144	s^{-1}	[18]
k_2	1.9×10^5	$M^{-1}\ s^{-1}$	[18]
V_{maxAcL}	9.58×10^{-5}	$pg\ s^{-1}\ \mu m^{-2}$	[8]
K_{mAcL}	0.405×10^{-3}	$pg\ \mu m^{-3}$	[8]
$a2c_H$_slope	1.5	–	[8]
$a2c_H$_thr	7	–	[8]
$c2a_H$_slope	1.5	–	[8]
$c2a_H$_thr	7	–	[8]
V_{maxNHE}	5.15×10^{-7}	$pg\ s^{-1}\ \mu m^{-2}$	Fit of data in[9]
K_{mNHE}	0.196×10^{-6}	M	Fit of data in[9]
h	2.67	–	Fit of data in[9]
λ_{NHE}	0.076	–	Fit of data in[9]
$pH_{0,NHE}$	7.1	–	Fit of data in[9]
$V_{maxTHCO3}$	2.02×10^{-5}	$pg\ s^{-1}\ \mu m^{-2}$	Fit of data in[19]
K_{mTHCO3}	7.38×10^{-3}	M	Fit of data in[19]
λ_{THCO3}	1.63	–	Fit of data in[9]
$pHe_{0,THCO3}$	6.85	–	Fit of data in[9]
γ_{THCO3}	4.2	–	Fit of data in[10]
$pHi_{0,THCO3}$	6.90	–	Fit of data in[10]
V_{maxCA9}	9.47×10^{-2}	$pg\ s^{-1}\ \mu m^{-2}$	[20]
K_{mCA9}	7.2×10^{-3}	M	[21]
δ_{CA9}	7.3	–	Fit of data in[22]

Table 1. Values of model parameters [a] AcL=lactic acid/lactate. [b] Parameter values have been determined and fixed as described in the Supplementary Material section

initial conditions discussed above, the simulations approach equilibrium quite fast and this indicates that the numerical solution of model equations is stable.

The model predictions for pH_i values in SCK cells grown in media with increasing acidity are shown in Fig. 3. We ran simulations with varying cell radius within a range of values which is reasonable for tumor cells, i.e. between 4.5 and 9 μm[24], and computed pH_i at equilibrium. As shown in Fig. 2 the numerical solutions approach equilibrium with slower kinetics for increasing cell radii. We chose a conservative criterion to define the equilibrium condition and we halted the simulations when $\Delta pH_i/\Delta t < 10^{-5}$ was reached. In these simulations, the volume of the environment was set to $V_c = 10^{12}\ \mu m^3 = 1$ ml, i.e. large enough to assure nearly constant pH_e values throughout the simulation runs. Figure 3 shows that model predictions are in excellent agreement with the experimental data.

Contribution of NHE and THCO3 transporters to pH_i in normoxic or hypoxic environments. We have used the model to study the biochemical mechanisms that allow tumor cells to survive to adverse environments. We have investigated the role of NHE and THCO3 transporters in the control of intracellular acidity by tumor cells exposed to normoxic or hypoxic environments. We ran several simulations by alternatively switching off the activity of NHE and THCO3 transporters, i.e. by setting the respective ν_{max} parameters to 0. The results are shown in Fig. 4 where we plot the pH_i values at equilibrium (see the previous section) as the function of environmental pH for cells grown under standard oxygen level or at 0.1 fraction thereof.

The simulations clearly show that under normoxic condition the contribution of the THCO3 transporter to pH_i is negligible. Under this condition pH_i is maintained to physiological levels thanks to the activity of NHE transporter that export H^+ ions outside the cells. On the contrary, THCO3 activity dominates in hypoxic environments.

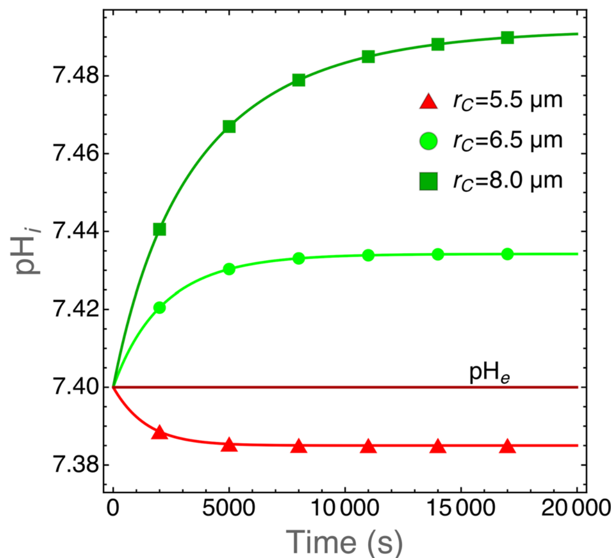

Figure 2. Plot of pH_i as the function of time for cells with the indicated cell radii. We take r_C values that are in the observed range for human tumor cells[24]. The model equations have been solved with the parameter values listed in Table 1. After an initial transient, pH_i reach an equilibrium at physiological values and this shows that the model (and its numerical solution) is stable and provides quantitative results in good agreement with actual experimental observations. We also plot pH_e for comparison. The extracellular pH does not vary because these runs were carried out for a limited time span and for cells growing in a large volume (1 mL) filled with fresh medium at physiological pH to mimic standard experimental conditions.

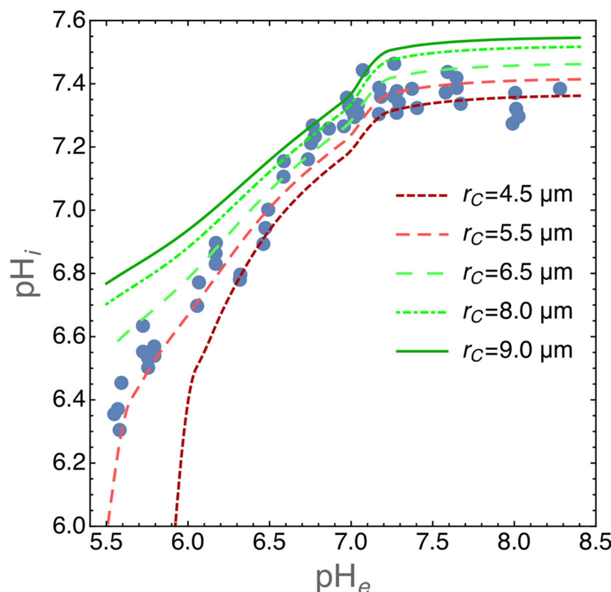

Figure 3. Plot of pH_i for SCK cells grown in media with different pH_e values. Experimental data have been redrawn from figure 2 in[23] (closed circles). The lines show pH_i values at equilibrium as predicted by our model for the indicated cell radii. It is important to note that these are not fits because our model does not have free parameters. Equilibrium was reached at $\Delta pH_i/\Delta t < 10^{-5}$. The volume of the environment was set at $V_c = 10^{12}\,\mu m^3 = 1ml$.

Role of Carbonic Anhydrase 9. As previously noted by Swietach et al.[11] pH_i regulation is not affected by CA9 expression in isolated tumor cells, but its role becomes important when cells are grown as three-dimensional aggregates (tumor spheroids). When expressed by cells grown as tumor spheroids CA9 induces a near uniform intracellular pH throughout the structure[11], an observation that was explained by diffusion-reaction modeling as follows: CA9 coordinates pH_i spatially by facilitating CO_2 diffusion in the unstirred extracellular space of the spheroid[11]. This intriguing conclusion, supported by experimental evidence, suggests that CA9

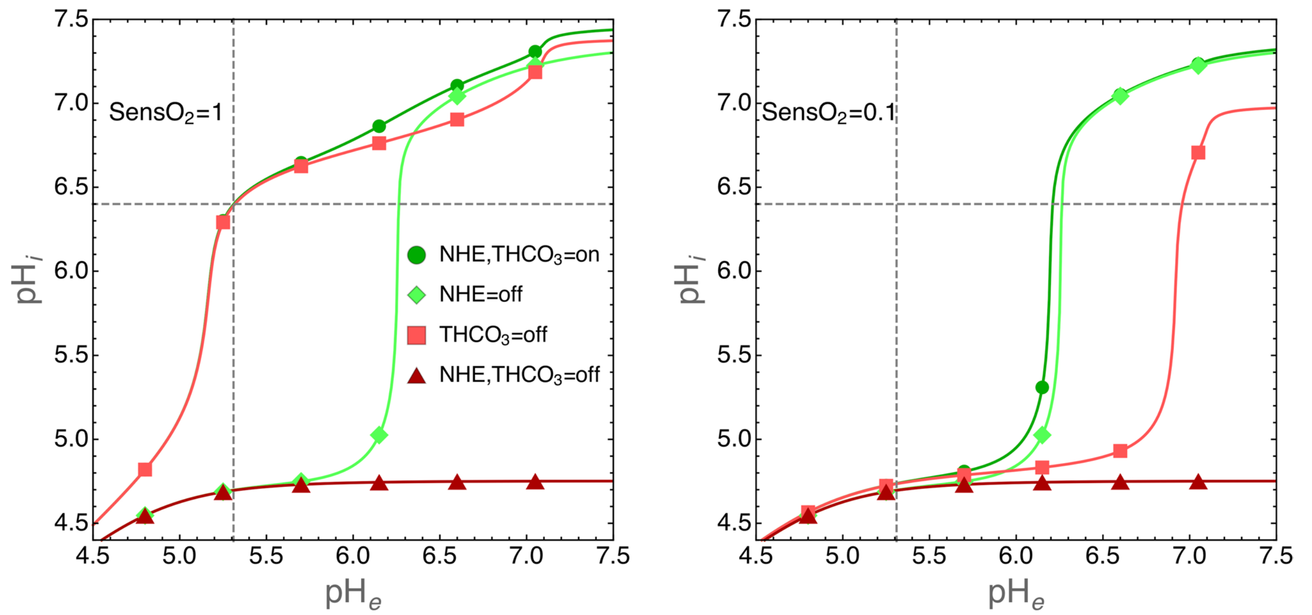

Figure 4. Contribution of NHE and THCO3 transporters to pH_i in normoxic (left panel) or hypoxic (right panel) environments. Simulations were run with the following parameters: cells radius $r_C = 6.5\,\mu m$ and environmental volume $V_c = 10^{12}\,\mu m^3$. The intracellular pH was calculated at equilibrium (see also the legend to Fig. 3) as the function of the indicated pH_e values. The activity of NHE and THCO3 transporters was switched off by setting the respective v_{max} parameters to 0. Environmental oxygen levels were tuned by setting the SensO2 parameter to 1 or to 0.1 (see the "Methods" section and the Supplementary Material for details). In both panels, dashed lines have been drawn to show the pH_e value at which $pH_i = 6.4$, a value largely compatible with cell life (see also the experimental data in Fig. 3 for a comparison).

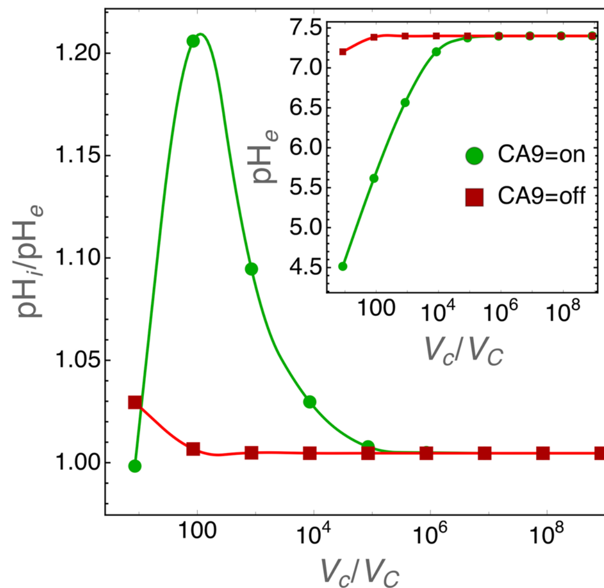

Figure 5. pH_i regulation by CA9 for decreasing size of the extracellular volume. Cell radius was set to the average size of 6.5 µm. The inset shows pH_e values and the main panel pH_i to pH_e ratio for varying V_c/V_C values (i.e. ratio of extracellular to cell volumes) when CA9 activity is turned on or off. In these simulations the extracellular environment is physically closed, i.e. the extracellular volume is unstirred and the diffusion of chemical species toward an "external reservoir" is not allowed.

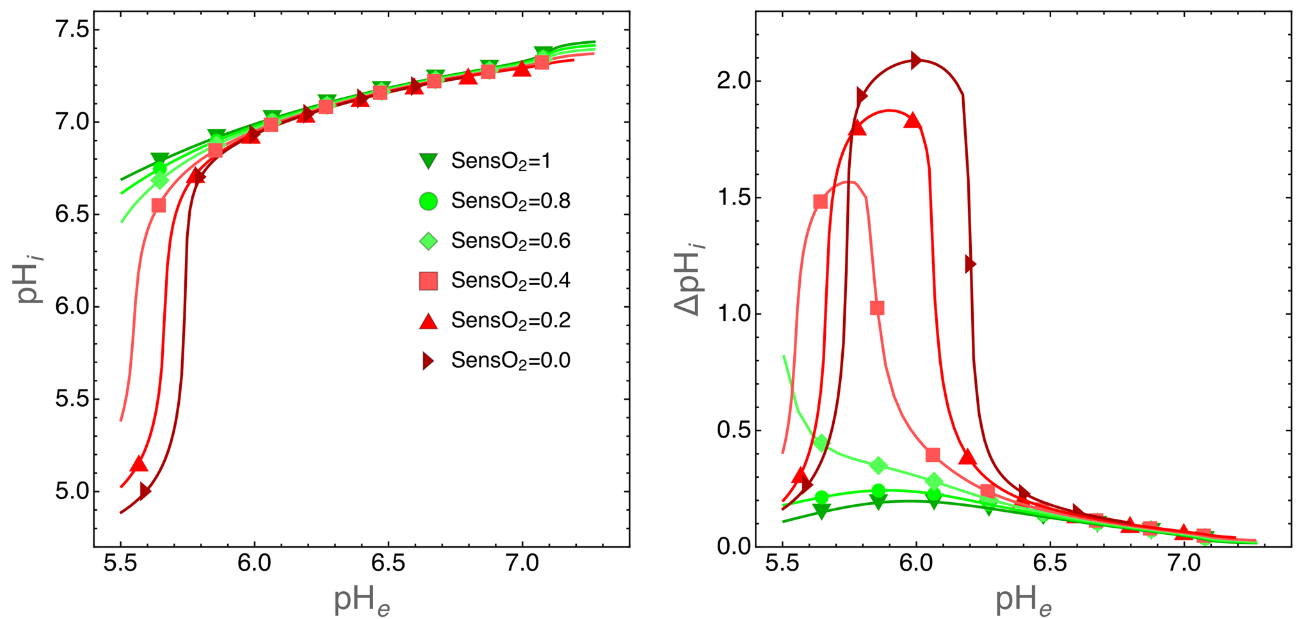

Figure 6. Role of CA9 on pH_i regulation for cells grown in a small environment with decreasing oxygen levels. In these simulations the extracellular volume was set to $V_c = 10^5\ \mu m^3$ and cell radius to $r_C = 6.5\ \mu m$ so that $V_c/V_C \approx 80$. Left panel: plot of pH_i at equilibrium as the function of pH_e for the indicated fractions of environmental O_2. Right panel: same simulations as those shown in the left panel, but here we plot $\Delta pH_i = pH_{i,CA9=on} - pH_{i,CA9=off}$, i.e. the difference in pH_i when CA9 is turned on or off. This plot clearly shows the nonlinear character of CA9 activity in the regulation of pH_i.

activity becomes important for the control of pH_i by tumor cells at critical sizes of the extracellular volume. We tested this hypothesis with our model, and the results are shown in Fig. 5.

The role of CA9 in pH_i regulation starts to become important at the extracellular to cell volume ratio $V_c/V_C \approx 10^4$ and reaches a maximum at $V_c/V_C \approx 100$. It is important to note that we simulated cells that grow in a closed environment. This means that at small extracellular volumes the acidity of the environment becomes too high and pH_i runs out of control (see also Fig. 4). However, the results in Fig. 5 show that when $V_c/V_C \approx 100$ and CA9 is active the extracellular pH at equilibrium is around 5.5 and $pH_i \approx 6.6$, well within the physiological range.

Simulations in Fig. 5 do not take into account the oxygen levels in the tumor environment. As discussed above (see the "Methods" section) CA9 expression is regulated by hypoxia[22] and thus it is interesting to investigate how pH_i is regulated by cells growing in small environments, i.e. when the CA9 role is not negligible, and when O_2 levels are lower and lower. Figure 6 shows that when $pH_e \geq 5.8$, CA9 acts as a nonlinear pH_i equalizer at any O_2 levels.

The model as a tool for exploratory data analysis. Germ-line mutations that inactivate the von Hippel-Lindau (*vhl*) gene cause the VHL syndrome, a rare inherited disorder characterized mainly, but not only, by renal cancers[25,26]. The VHL protein drives ubiquitination and finally degradation of the hypoxia-inducible factor alpha (HIF) which in turn regulates a number of intracellular pathways that collectively confer resistance to hypoxia to cancer cells[25,26]. However, experimental findings suggest that both HIF-dependent and HIF-independent mechanisms are essential for VHL-mediated tumor suppressor effects[25,26].

Stable transfection of 786-O renal cancer cells with a full-length human *vhl* gene significantly decreased proton and bicarbonate fluxes with respect to *vhl*-null cells in spite of increased or unaltered expression of ion transporters[27]. In particular, experiments showed that the rate of pH_i change (dpH_i/dt) upon alkali or acid load was reduced to $\sim 25-45\%$ in VHL^+ cells with respect to VHL^- cells. A number of control experiments were carried out to test possible effects of VHL proteins in these cells, but the effects of VHL protein on ion fluxes remained unexplained[27]. Here we modify our model to provide a possible interpretation of these experimental observations.

In the experiments with VHL^+ and VHL^- cells, proton fluxes were measured in cells exposed to Cl^--deprived solutions, during recovery from NH_4^+-induced cell acidification or subjected to hypertonic shock[27]. Simulations of NH_4^+-induced cell acidification and hypertonic shock would require major revision of the model to include a number of chemical, biochemical and morphological details such as, e.g., NH_4Cl dissociation kinetics and intra- and extracellular flows of all involved ionic species, cell volume dynamics during osmotic shock and a detailed description of how cell shrinkage and swelling activate ions transport. In addition, quantitative information which is required to set the values of specific model parameters is not fully available, further hampering the development of specific detailed models. We therefore focus on cell treatments with Cl^--deprived solutions.

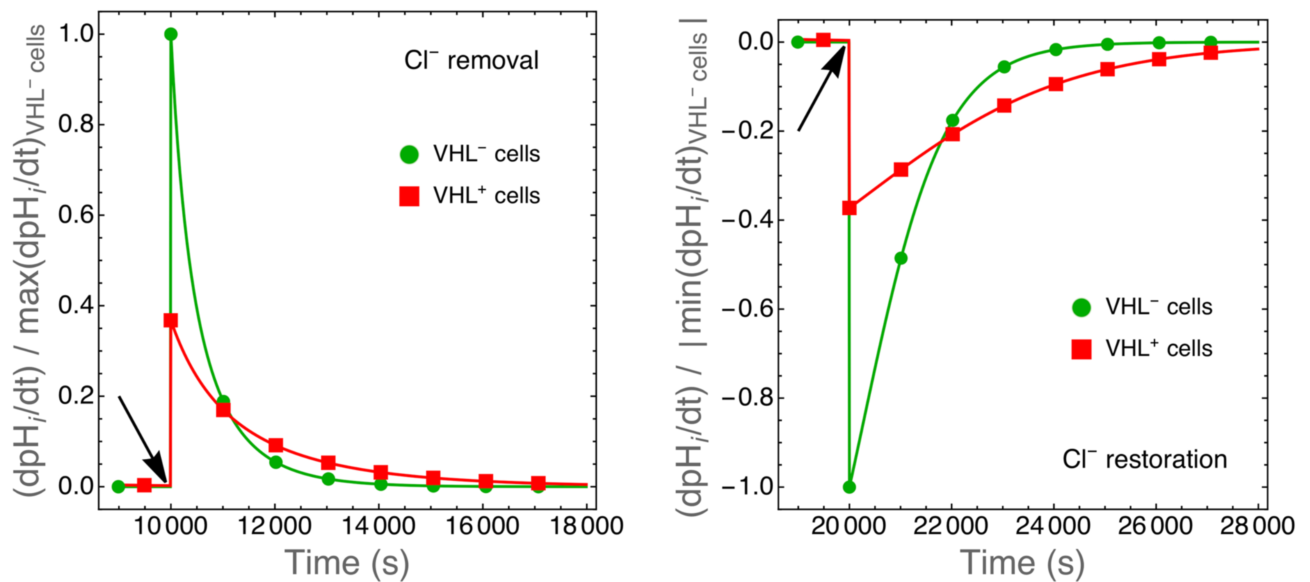

Figure 7. Rate of intracellular pH change in simulated VHL^- and VHL^+ cells upon removal (left panel) and restoration (right panel) of environmental Cl^- anions. Values have been normalized with respect to the maximum (left panel) or to the absolute value of the minimum (right panel) rate of pH_i change calculated for VHL^- cells. Simulations were run until pH_i reached equilibrium. Cl^- removal or restoration was modeled by suddenly (arrows) switching to 0 or to normal values, respectively, the rate of HCO3$^-$ efflux (Eq. 8, see the "Methods" section) as described in the text. The initial rate of pH_i change in VHL^+ is reduced to ∼ 40% of that of VHL^- cells as observed in actual experiments.

The rationale behind cell treatment with Cl^--deprived solutions was the discovery that VHL expression in 786-O renal cancer cells increased mRNA and protein levels of Cl^-/HCO_3^- AE2 anion exchanger by 3.5 fold, although the apparent cell surface expression of AE2 was similar in VHL^+ and VHL^- cells as evaluated by immunostaining[27]. The AE2 transporter exchange Cl^- with HCO_3^-, and when the cells are exposed to Cl^- -deprived solutions Cl^- can only exit from the cells thus forcing HCO_3^- import[27]. In other words, the treatment makes an otherwise bidirectional transport unidirectional. Our simplified model takes into account only a generic unidirectional transporter that shuttle HCO_3^- from the environment into the cell and that is described by Eq. 6 (see the "Methods" section). To model the AE2 exchanger we introduce one more equation to describe also the rate of HCO_3^- efflux (see Eq. 8 in the "Methods" section). We then perturbed the system at equilibrium by suddenly switching to 0 the rate of HCO_3^- efflux to model cells placed in Cl^--deprived baths or switching it to normal values to model cells re-placed under standard environmental conditions (see Fig. 7).

The expression of many genes is altered in VHL^+ cells and VHL protein is known to affect several physiologic pathways[28]. Quantitative data are not fully available and therefore it is impossible with the present knowledge to reproduce the whole complex phenotype of these cells *in silico*. However, we note that among the physiologic pathways altered in 786-O cells expressing VHL proteins glycolysis and respiration are prominent[28]. Glycolysis was observed to be approximately one half of that measured for VHL^- cells, a finding that was paralleled by a corresponding two fold downmodulation of glucose transporters, whereas respiration was found to be increased by a factor of two[28]. VHL expression was also observed to dramatically reduce (i.e. a $\sim 80 - 100$-fold change) lactate transport in other cell systems[29]. Our model can easily take into account the phenotype of VHL^+ cells as far as these pathways are concerned. We multiplied specific rates by appropriate factors: the rate of proton production (gH^+ in Eq. 11) was divided by 2 to model the reduced lactate/H^+ production by glycolysis; the rate of CO_2 production (gCO_2 in Eq. 11) was multiplied by 2 to model the increased respiration rate; finally the maximum rate of lactate transport through MCT transporters (ν_{maxMCT} in Eq. 2) was divided by 80 to model the observed reduction of lactate transport.

The simulations show that the initial rate of intracellular pH change (dpH_i/dt) is reduced to ∼ 40% in VHL^+ cells with respect to VHL^- cells (Fig. 7) in agreement with experimental observations[27]. As shown in Fig. 8, a reduced glycolytic rate is mainly responsible for this effect. This shows that the present model, although simplified, can still be adapted to simulate different cell phenotypes and used to suggest novel interpretation of otherwise paradoxical[27] and yet unexplained experimental observations.

Discussion

We have developed a biophysical model to explore the complex molecular mechanisms that allow tumor cells to regulate both intracellular and extracellular acidity, but we are not alone, other modeling efforts have tried to capture the essential features of the biochemical pathways that lead to acid homeostasis in tumor cells (see e.g.[30–33]). We have taken the remarkable models described in[32] and[33] as our starting point, because of their direct applicability to the analysis of experimental data. The former provides a fully tractable quantitative description of the interplay between H^+ and HCO_3^- transporters with Na^+/K^+-ATPase and Na^+, K^+ and Cl^- ion fluxes, while

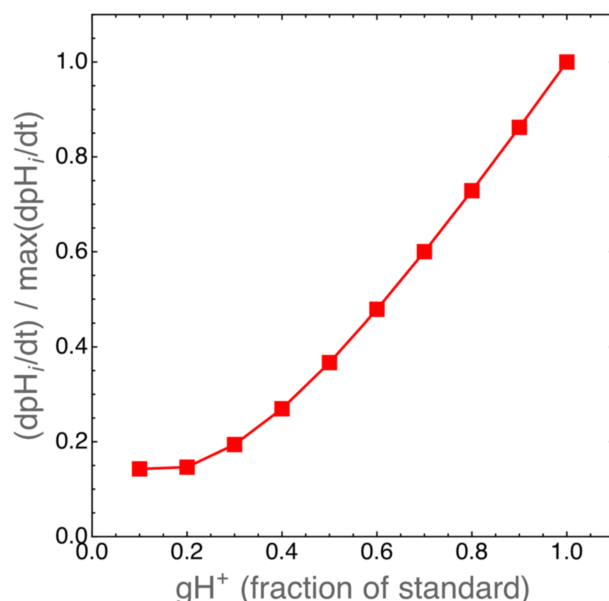

Figure 8. Reduced glycolytic rates in VHL^+ cells might explain the effect shown in Fig. 7. VHL protein expression was observed to downmodulate the expression of glucose transporters and to reduce the glycolytic rate, and hence lactate/H^+ production, in renal cancer cells[28]. Here we plot the rate of pH_i change in simulated VHL^+ cells as the function of proton production rate through glycolysis (rate gH^+ in Eq. 11, see the "Methods" section and the Supplementary material). The standard value of gH^+ is calculated (see Eq. 11) as $gAcL \cdot (MW_H/MW_{AcL})$ where the value of gAcl is given in Table 1. When $gH^+ = 1$, dpH_i/dt in VHL^+ cells is equal to that of VHL^- cells.

the latter investigates the interaction of MCT transporters and CA9. We go a few steps further and model the network of important paths that connect together cell metabolism and hypoxia with transport of H^+ and HCO_3^- ions and CA9 activity (see Fig. 1). The coupling of ion transport mechanisms with metabolism and hypoxia is essential if we want to understand how tumor cells grow and shape their microenvironment, an interplay that is of fundamental importance for the adaptation and evolution of cancer cells within a solid tumor. As mentioned at the beginning of the Results section, we have developed a computer program that successfully reproduces the growth and the behavior of tumor cells in both liquid and solid cancers[6–8]. It is a lattice-free model that contains a rather detailed description of tumor cell metabolism and of the cell cycle, as well as many other biochemical and biophysical features (e.g. cell mechanics, cell division, etc.)[6–8]. This has already allowed us to characterize new biophysical properties of tumors and of their microenvironment[34–37], but the program still contains an excindingly simplified description of how cells control their intracellular pH. The program has an incremental structure, and we add new parts as soon as they are independently validated. The present model is one of these parts, and once integrated in our previous software it will further increase its descriptive and predictive potential. We hope in this way to understand key biological features such as cell adaptation and evolution in tumor microenvironments and explore important aspects such as tumor cell resistance to therapies. Here we show that the present model can nonetheless be used as a tool for exploratory data analysis and for quantitative purposes.

We remark that with the model described here we are able to give a quantitative assessment of the importance of specific molecular mechanisms. For instance, simulations show that H^+ efflux from tumor cells dominates the control of intracellular acidity in normoxic environments, whereas HCO_3^- import in hypoxic tumor areas (in our simulation where the fraction of oxygen decrease to 0.1 of standard values). Experiments have shown that in *in vivo* tumor micro-environments oxygen reaches 10% of its normal value at a distance of $\approx 150\,\mu m$, i.e. ≈ 10 cell diameters, from blood vessels[38]. Thus, within this short distance the control of pH_i is attained by tumor cells through a switch from H^+ export to HCO_3^- import pathways. This observation gives further support to recent work that has shown that inhibition of HCO_3^- fluxes inhibits the growth of experimental tumors by increasing intracellular acidity and cell death[39]. When we recall that the hypoxic regions are those where tumor cells show higher resistance to therapies, such as e.g. radiotherapy, then we see that approaches that aim at inhibiting HCO_3^- fluxes would target the very cells that colonize the inner tumor regions and that would otherwise be resistant to therapies, and improve cancer control.

Finally, the model singles out the important role of CA9. The simulations show that CA9 acts as a nonlinear pH_i equalizer at any O_2 level in cells that grow in acidic extracellular environments. This result is in agreement with the experimental observations by Swietach and colleagues[11], collected with tumor spheroids. They observed near-uniform pH_i values throughout the spheroid structure due to CA9 activity in spheroids grown up to $\approx 500\,\mu m$ diameter. It has long been recognized that tumor spheroids of this size show steep gradients of oxygen with fractions that go as far down as 0 at the center of the spheroid[40]. Our simulations show that this is due to the concerted action of CA9 and of hypoxia that up-regulates CA9 expression. These two mechanisms

collectively help cells to keep their intracellular pH under control because of increased HCO_3^- production followed by HCO_3^- import through THCO3 transporters.

Conclusion

While tumor cell adaptation and survival to extreme microenvironments are key concepts in oncogenesis[1–3], we remark that acid homeostasis is central to cellular adaptation in a much wider context. Active transport of acid/base equivalents across cell membranes into the extracellular spaces may cause transient and rapid changes of microenvironmental and cellular pHs like those observed for other ions involved in cell signalling. Indeed, pH transients have been shown to be important in intra- and inter-cellular communication in the nervous system and are known to affect a number of essential functions, like e.g. neuronal excitability and synaptic transmission[41]. This in turn implies that animal cells could sense and adapt to pH changes. The underlying molecular mechanisms are still not well understood, but the role of G-protein coupled receptors in proton sensing is increasingly investigated also in relation to pathological conditions, besides cancer, that result in an increased extracellular acidity, such as infarction and inflammation[42]. We conclude that our model can be used as an essential building block of more comprehensive *in silico* research on solid tumors[43], but it may also help understanding how other cells can sense and dynamically adapt to pH changes.

Methods

Bicarbonate buffer and initial conditions. Central to the whole scheme of reactions shown in Fig. 1 is the hydration of CO_2. It is well known that at physiologic temperature (i.e. $\sim 37\,^\circ C$) carbonic acid dissociates very quickly and represents less than 0.5% of the total carbon dioxide and bicarbonate ion[44]. Thus, the hydration of CO_2 can be approximated by the following chemical reaction:

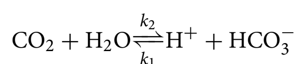

$$CO_2 + H_2O \underset{k_1}{\overset{k_2}{\rightleftharpoons}} H^+ + HCO_3^-$$

The values of the two rate constants k_1 and k_2 have been determined in cells under standard culture conditions in two independent experiments with good agreement[11,18]. We take the values in[18]: $k_1 \simeq 0.144\,s^{-1}$ and $k_2 \simeq 1.9 \cdot 10^5\,M^{-1}\,s^{-1}$.

We compare model outputs with experimental data obtained with cell cultures *in vitro*, in a standard atmosphere at 37 °C and 5% CO_2 at 1 atm pressure. To compute the initial density of CO_2 dissolved in water under these conditions we use Henry's law $c = k(T)P$ where c is the molar concentration of the gas in water, P the pressure and $k(T)$ is a function of temperature

$$k(T) = k^\Theta \exp\left[-\frac{\Delta_{\rm sol}\,k}{R}\left(\frac{1}{T} - \frac{1}{T^\Theta}\right)\right]$$

with $T^\Theta = 298.15\,K$, $k^\Theta = 3.3 \cdot 10^{-4}$mol m^{-3} Pa^{-1}and $-\frac{\Delta_{\rm sol}\,k}{R} = 2400\,K$ (see ref.[45] for further details); we find that the initial density of CO_2 in cell medium under standard culture conditions is:

$$\rho_{CO_2} = 5.39 \cdot 10^{-5}\,\frac{\rm pg}{\mu m^3}$$

Finally, given the CO_2 concentration we find the density of HCO_3^- ions from the Henderson-Hasselbach equation:

$$\mathrm{pH} = \mathrm{pKa} + \log_{10}\left(\frac{[HCO_3^-]}{[CO_2]}\right)$$

where $\mathrm{pKa} = -\log_{10}(k_1/k_2) \simeq 6.12$.

Where not otherwise specified, we fixed the standard intracellular and extracellular pH at 7.4, which determines the initial value of the molar concentration of H^+ ions inside and outside the cells.

CO_2 diffusion through the cell membrane. Given the assumptions above, the component of CO_2 normal to the cell membrane is described by the Fick's first law:

$$J_{1\to 2} = -P_{M,CO_2} \cdot (C_2 - C_1)$$

where $J_{1\to 2}$ is the flux from 1 to 2 in units of concentration over time and surface area S_C, P_{M,CO_2} is the permeability of the carbon dioxide and C_i is the concentration of CO_2 in the i-th volume. Since we model cells grown in an incubator at constant CO_2 pressure, the CO_2 concentration can reach values far from equilibrium only inside cells because of the oxygen consumption by cell metabolism and of the equivalent CO_2 production. This means that in the present model there is only a net outward flux of carbon dioxide from cells to the environment. Thus, the net flux of CO_2 due to diffusion is:

$$\left.\frac{dm_{CO_2,C}}{dt}\right|_{\rm diff} = -J_{1\to 2} \cdot MW_{CO_2} \cdot S_C = P_{M,CO_2}\left(\frac{m_{CO_2,c}}{V_c} - \frac{m_{CO_2,C}}{V_C}\right)S_C \qquad (1)$$

MCT transporters. The MCTs are a family of bidirectional H^+ and lactate co-transporters expressed at the cell membrane and their activity has been shown to depend on the pH values on both sides of the cell membrane

(see refs.[6–8] and references therein). We model their activity with parameter values extrapolated from experimental observations[6–8] and we use the following equations and parameters to describe the rate of transport of H^+ inside and outside the cell:

$$\begin{aligned} \nu_{\mathrm{MCT}}^{\mathrm{out}\to\mathrm{in}} &= \mathrm{a2c_H} \cdot \frac{\nu_{\mathrm{maxMCT}} \cdot m_{\mathrm{H^+,c}}}{V_c K_{\mathrm{mMCT}} + m_{\mathrm{H^+,c}}} \\ \nu_{\mathrm{MCT}}^{\mathrm{in}\to\mathrm{out}} &= \mathrm{c2a_H} \cdot \frac{\nu_{\mathrm{maxMCT}} \cdot m_{\mathrm{H^+,C}}}{V_C K_{\mathrm{mMCT}} + m_{\mathrm{H^+,C}}} \end{aligned} \tag{2}$$

where $\nu_{\mathrm{maxMCT}} = V_{\mathrm{maxAcL}} \cdot \frac{\mathrm{MW_H}}{\mathrm{MW_{AcL}}} \cdot S_C$, $K_{\mathrm{mMCT}} = K_{\mathrm{mAcL}} \cdot \frac{\mathrm{MW_H}}{\mathrm{MW_{AcL}}}$ and where the ratio of molecular weights is used to rescale the equations from concentrations to masses.

In Eq. 2, $\mathrm{a2c_H}$ and $\mathrm{c2a_H}$ depend, respectively, on extracellular and intracellular pH, and phenomenologically describe the dependency of MCT transport activity on acidity (for a complete analysis see[6–8]):

$$\begin{aligned} \mathrm{a2c_H} &= 2 - \tanh(\mathrm{a2c_{H_slope}} \cdot \mathrm{pH}_c - \mathrm{a2c_{H_thr}}) \\ \mathrm{c2a_H} &= 2 - \tanh(\mathrm{c2a_{H_slope}} \cdot \mathrm{pH}_C - \mathrm{c2a_{H_thr}}) \end{aligned} \tag{3}$$

NHE transporters. Sodium-hydrogen exchangers (NHE) are membrane transport proteins that exploit the influx of Na^+ to export H^+ ions. The sodium concentration gradient is maintained by the ATP-dependent Na^+/K^+ pump[19,46] so that the activity of NHE indirectly depends on ATP availability. This implies that as long as ATP is available the flux of H^+ due to NHE is essentially unidirectional. It has also been reported that NHE activity is inhibited by hypoxia[10,19] and that, in the long-term, hypoxia inhibits the expression of NHE proteins. Energy and oxygen tune NHE activity and as in the previous model of tumor cell metabolism and growth[6–8], here we take into account these regulatory circuits by means of the two variables SensATP and $\mathrm{SensO_2}$ that assume real values in the interval [0, 1].

Experimental observations indicate that NHE activity is described by a Hill equation[9,47,48] and hence the unidirectional flux of H^+ from the cell to the environment due to NHE transport is modeled by the equation:

$$\nu_{\mathrm{NHE}}^{\mathrm{in}\to\mathrm{out}} = \mathrm{SensATP} \cdot \mathrm{SensO_2} \cdot \mathrm{fpHe_{NHE}} \cdot \frac{\nu_{\mathrm{maxNHE}} \cdot m_{\mathrm{H^+,C}}^h}{(V_C \cdot \mathrm{MW_H} \cdot K_{\mathrm{mNHE}})^h + m_{\mathrm{H^+,C}}^h} \tag{4}$$

where $\nu_{\mathrm{maxNHE}} = \mathrm{V_{maxNHE}} \cdot S_C$ and $\mathrm{fpHe_{NHE}}$ is a phenomenological function that tunes the activity of NHE transport as a function of extracellular pH:

$$\mathrm{fpHe} = \frac{1}{2}\left(1 + \frac{\mathrm{pH_e} - \mathrm{pH_0}}{\lambda + |\mathrm{pH_e} - \mathrm{pH_0}|}\right) \tag{5}$$

Indeed, it has been observed that extracellular acidity enhances H^+ transport through NHE[9,19,49]. In the Supplementary Material we discuss how we fix parameter values and define the function fPHe on the basis of experimental observations.

Transport of bicarbonate ions. As discussed above, we model the activity of a generic bicarbonate ion importer (THCO3). The Na^+-dependent Cl^-/HCO_3^- exchanger appears to dominate HCO_3^- fluxes in tumor cells[9,10], and therefore we take this transporter as a reference to set the values of parameters and fix general biochemical characteristics. This is an important part of the model, because it has been shown that tumor cells do actively import HCO_3^- ions to buffer their internal pH[9,10], and that this is a common property of different cancer cells. Experimental studies have demonstrated that HCO_3^- import is regulated by both intracellular and extracellular pH but not by hypoxia and that the transport follows a simple Michaelis-Menten kinetics. In the scientific literature there are no indications, as far as we can tell, that HCO_3^- transport depends on ATP availability. However, just as observed for proton export by NHE transporters, HCO_3^- transport proceeds by parallel fluxes of ions, like Na^+ and Cl^-, along their electrochemical gradients that are actively maintained by cells through energy-consuming paths. Thus, it is likely that even HCO_3^- transport is controlled by ATP availability, albeit indirectly. On the basis of these considerations we model HCO_3^- import as follows:

$$\nu_{\mathrm{THCO3}}^{\mathrm{out}\to\mathrm{in}} = \mathrm{SensATP} \cdot \mathrm{fpHe_{THCO3}} \cdot \mathrm{fpHi_{THCO3}} \cdot \frac{\nu_{\mathrm{maxTHCO3}} \cdot m_{\mathrm{HCO_3^-,c}}}{V_c \cdot \mathrm{MW_{HCO3}} \cdot K_{\mathrm{mHCO3}} + m_{\mathrm{HCO_3^-,c}}} \tag{6}$$

where $\nu_{\mathrm{maxTHCO3}} = \mathrm{V_{maxTHCO3}} \cdot S_C$ and the two functions $\mathrm{fpHe_{THCO3}}$ and $\mathrm{fpHi_{THCO3}}$ phenomenologically describe how HCO_3^- import is affected by extracellular and intracellular pH, respectively. These functions have been fit to actual experimental data (see the Supplementary Material) and are modeled by the following equations:

$$\begin{aligned} \mathrm{fpHi_{THCO3}} &= \frac{1}{2}\{1 + \tanh[\gamma_{\mathrm{THCO3}} \cdot (\mathrm{pHi_{0,THCO3}} - \mathrm{pH_i})]\} \\ \mathrm{fpHe_{THCO3}} &= \frac{1}{2}\{1 + \tanh[\lambda_{\mathrm{THCO3}} \cdot (\mathrm{pH_e} - \mathrm{pHe_{0,THCO3}})]\} \end{aligned} \tag{7}$$

In *in silico* experiments with VHL^+ and VHL^- cells we make HCO_3^- transport bidirectional by considering HCO_3^- efflux from cells as follows:

$$\nu_{\text{THCO3}}^{\text{in}\to\text{out}} = \text{SensATP} \cdot \text{fpHe}_{\text{THCO3}} \cdot \text{fpHi}_{\text{THCO3}} \cdot \frac{\nu_{\text{maxTHCO3}} \cdot m_{\text{HCO}_3^-,\text{C}}}{V_C \cdot \text{MW}_{\text{HCO3}} \cdot K_{\text{mHCO3}} + m_{\text{HCO}_3^-,\text{C}}} \tag{8}$$

Activity of Carbonic Anhydrase 9. The enzyme CA9 is expressed by cells of many different solid tumors, and in general its expression correlates with cancer aggressiveness and poor therapeutic outcome[11–13]. It is a membrane-tethered enzyme and it is mainly found at the external surface of cells where it catalyses the hydration of CO_2[11–13]. Importantly, its expression is regulated by hypoxia and indeed CA9 is a marker of hypoxia[22]. Again, experimental observations show that CA9 activity follows a Michaelis-Menten kinetics. Thus:

$$\nu_{\text{CA9}} = \text{h}_{\text{CA9}} \cdot \frac{\nu_{\text{maxCA9}} \cdot m_{\text{CO}_2,\text{c}}}{V_c \cdot \text{MW}_{\text{CO2}} \cdot K_{\text{mCA9}} + m_{\text{CO}_2,\text{c}}} \tag{9}$$

where where $\nu_{\text{maxCA9}} = \text{V}_{\text{maxCA9}} \cdot S_C$ and h_{CA9} is a phenomenological functions that describe how hypoxia tunes CA9 expression:

$$\text{h}_{\text{CA9}} = 3 + 2 \cdot \tanh\left(-\delta_{\text{CA9}} \cdot \text{SensO2}\right) \tag{10}$$

This is a function of the fraction of available oxygen which, in our model, is defined by SensO2, and it describes the fold change in CA9 expression as observed in actual experiments (see the Supplementary Material).

The full model and its numerical integration. The full model is represented by the following set of differential equations:

$$\begin{aligned}
\frac{dm_{\text{CO}_2,\text{C}}}{dt} &= \text{gCO}_2 - k_1 \cdot m_{\text{CO}_2,\text{C}} + k_2 \cdot m_{\text{H}^+,\text{C}} \cdot m_{\text{HCO}_3^-,\text{C}} \cdot \frac{10^3 \cdot \text{MW}_{\text{CO}_2}}{V_C \cdot \text{MW}_{\text{H}} \cdot \text{MW}_{\text{HCO3}}} - J_{C\to c} \cdot S_C \cdot \text{MW}_{\text{CO}_2} \\
\frac{dm_{\text{H}^+,\text{C}}}{dt} &= \text{gH}^+ + k_1 \cdot m_{\text{CO}_2,\text{C}} \cdot \frac{\text{MW}_{\text{H}}}{\text{MW}_{\text{CO}_2}} - k_2 \cdot m_{\text{H}^+,\text{C}} \cdot m_{\text{HCO}_3^-,\text{C}} \cdot \frac{10^3}{V_C \cdot \text{MW}_{\text{HCO3}}} \\
&\quad - \nu_{\text{MCT}}^{\text{in}\to\text{out}} + \nu_{\text{MCT}}^{\text{out}\to\text{in}} - \nu_{\text{NHE}}^{\text{in}\to\text{out}} \\
\frac{m_{\text{HCO}_3^-,\text{C}}}{dt} &= k_1 \cdot m_{\text{CO}_2,\text{C}} \cdot \frac{\text{MW}_{\text{HCO3}}}{\text{MW}_{\text{CO}_2}} - k_2 \cdot m_{\text{H}^+,\text{C}} \cdot m_{\text{HCO}_3^-,\text{C}} \cdot \frac{10^3}{V_C \cdot \text{MW}_{\text{H}}} + \nu_{\text{THCO3}}^{\text{out}\to\text{in}} \\
\frac{dm_{\text{CO}_2,\text{c}}}{dt} &= 0 \\
\frac{dm_{\text{H}^+,\text{c}}}{dt} &= k_1 \cdot m_{\text{CO}_2,\text{c}} \cdot \frac{\text{MW}_{\text{H}}}{\text{MW}_{\text{CO}_2}} - k_2 \cdot m_{\text{H}^+,\text{c}} \cdot m_{\text{HCO}_3^-,\text{c}} \cdot \frac{10^3}{V_c \cdot \text{MW}_{\text{HCO3}}} + \nu_{\text{MCT}}^{\text{in}\to\text{out}} - \nu_{\text{MCT}}^{\text{out}\to\text{in}} \\
&\quad + \nu_{\text{NHE}}^{\text{in}\to\text{out}} + \nu_{\text{CA9}} \cdot \frac{\text{MW}_{\text{H}}}{\text{MW}_{\text{CO}_2}} \\
\frac{m_{\text{HCO}_3^-,\text{c}}}{dt} &= k_1 \cdot m_{\text{CO}_2,\text{c}} \cdot \frac{\text{MW}_{\text{HCO3}}}{\text{MW}_{\text{CO}_2}} - k_2 \cdot m_{\text{H}^+,\text{c}} \cdot m_{\text{HCO}_3^-,\text{c}} \cdot \frac{10^3}{V_c \cdot \text{MW}_{\text{H}}} - \nu_{\text{THCO3}}^{\text{out}\to\text{in}} \\
&\quad + \nu_{\text{CA9}} \cdot \frac{\text{MW}_{\text{HCO3}}}{\text{MW}_{\text{CO}_2}}
\end{aligned} \tag{11}$$

where $\text{gH}^+ = \text{gAcL} \cdot \text{MW}_{\text{H}}/\text{MW}_{\text{AcL}}$ and $\text{gCO}_2 = \text{qO}_2 \cdot \text{MW}_{\text{CO}_2}/\text{MW}_{\text{O}_2}$ are, respectively, the rates of H^+ and CO_2 production that are proportional to the rate of lactate production gAcL and oxygen consumption qO_2 as defined in our previous work[6–8], and all the other rates, and regulatory functions, are given in equations 1–10. The multiplicative factor 10^3 that appears in the right-hand side of equations 11 above comes from the conversion of standard molar concentration units to the units used here where masses are expressed in pg and volumes in μm^3.

In *in silico* experiments with VHL^+ and VHL^- cells, where HCO_3^- transport is bidirectional, the differential equations in the set 11 that describe HCO_3^- kinetics were modified as follows:

$$\begin{aligned}
\frac{m_{\text{HCO}_3^-,\text{C}}}{dt} &= k_1 \cdot m_{\text{CO}_2,\text{C}} \cdot \frac{\text{MW}_{\text{HCO3}}}{\text{MW}_{\text{CO}_2}} - k_2 \cdot m_{\text{H}^+,\text{C}} \cdot m_{\text{HCO}_3^-,\text{C}} \cdot \frac{10^3}{V_C \cdot \text{MW}_{\text{H}}} + \nu_{\text{THCO3}}^{\text{out}\to\text{in}} - \nu_{\text{THCO3}}^{\text{in}\to\text{out}} \\
\frac{m_{\text{HCO}_3^-,\text{c}}}{dt} &= k_1 \cdot m_{\text{CO}_2,\text{c}} \cdot \frac{\text{MW}_{\text{HCO3}}}{\text{MW}_{\text{CO}_2}} - k_2 \cdot m_{\text{H}^+,\text{c}} \cdot m_{\text{HCO}_3^-,\text{c}} \cdot \frac{10^3}{V_c \cdot \text{MW}_{\text{H}}} - \nu_{\text{THCO3}}^{\text{out}\to\text{in}} + \nu_{\text{THCO3}}^{\text{in}\to\text{out}} \\
&\quad + \nu_{\text{CA9}} \cdot \frac{\text{MW}_{\text{HCO3}}}{\text{MW}_{\text{CO}_2}}
\end{aligned}$$

The system of differential equations 11 is nonlinear and stiff because it incorporates processes with different kinetics, from the fast kinetics of CO_2 hydration and diffusion to the relatively slow kinetics of ion transport and enzyme activity. The system cannot be solved analytically and appropriate numerical approaches are required. We previously investigated this aspect within the context of complex large-scale biophysical models[50] and found that the implicit Euler method is well-suited for the numerical integration of models of this kind. We solved the discretized system of differential equation 11 using the implicit Euler algorithm followed by the Newton-Raphson method to solve numerically the resulting system of nonlinear equations. The code has been implemented in C++

using the computational framework provided by the GNU Scientific Library[51]. We used the standard Newton-Raphson solver *gsl_multiroot_fsolver_dnewton* and the *gsl_multiroot_test_residual* library to test the convergence of the algorithm (threshold $\epsilon < 10^{-6}$) within a maximum number of iterations fixed at $N_{\max} = 1000$.

Received: 22 May 2020; Accepted: 28 July 2020
Published online: 12 August 2020

References

1. Swietach, P., Vaughan-Jones, R. D., Harris, A. L. & Hulikova, A. The chemistry, physiology and pathology of pH in cancer. *Philos. Trans. R. Soc. B* **369**, 20130099 (2014).
2. Estrella, V. *et al.* Acidity generated by the tumor microenvironment drives local invasion. *Cancer Res.* **73**, 1524–1535 (2013).
3. Corbet, C. & Feron, O. Tumour acidosis: From the passenger to the driver's seat. *Nat. Rev. Cancer* **17**, 577–593 (2017).
4. Korenchan, D. E. & Flavell, R. R. Spatiotemporal pH heterogeneity as a promoter of cancer progression and therapeutic resistance. *Cancers* **11**, 1026–2069 (2019).
5. Fang, J. S., Gillies, R. D. & Gatenby, R. A. Adaptation to hypoxia and acidosis in carcinogenesis and tumor progression. *Semin. Cancer Biol.* **18**, 330–337 (2008).
6. Chignola, R. & Milotti, E. A phenomenological approach to the simulation of metabolism and proliferation dynamics of large tumour cell populations. *Phys. Biol.* **2**, 8–22 (2005).
7. Chignola, R., Delfabbro, A., Dalla Pellegrina, C. & Milotti, E. Ab initio phenomenological simulation of the growth of large tumor cell populations. *Phys. Biol.* **4**, 114–133 (2007).
8. Milotti, E. & Chignola, R. Emergent properties of tumor microenvironment in a real-life model of multicell tumor spheroids. *PLoS ONE* **5**, e13942 (2010).
9. Hulikova, A., Vaughan-Jones, R. D. & Swietach, P. Dual role of CO_2/HCO_3^- buffer in the regulation of intracellular pH of three-dimensional tumor growths. *J. Biol. Chem.* **286**, 13815–13826 (2011).
10. Hulikova, A., Harris, A. L., Vaughan-Jones, R. D. & Swietach, P. Regulation of intracellular pH in cancer cell lines under normoxia and hypoxia. *J. Cell. Physiol.* **228**, 743–752 (2013).
11. Swietach, P. *et al.* Tumor-associated carbonic anhydrase 9 spatially coordinates intracellular pH in three-dimensional multicellular growths. *J. Biol. Chem.* **283**, 20473–20483 (2008).
12. Swietach, P., Vaughan-Jones, R. D. & Harris, A. L. Regulation of tumor pH and the role of carbonic anhydrase 9. *Cancer Metastasis Rev.* **26**, 299–310 (2007).
13. Span, P., Bussink, J., Manders, P., Beex, L. & Sweep, C. Carbonic anhydrase-9 expression levels and prognosis in human breast cancer: association with treatment outcome. *Br. J. Cancer* **89**, 271–276 (2013).
14. McIntyre, A. *et al.* Carbonic Anhydrase IX promotes tumor growth and necrosis in vivo and inhibition enhances anti-VEGF therapy. *Clin. Cancer Res.* **18**, 3100–3111 (2012).
15. Khalifah, R. G. The carbon dioxide hydration activity of Carbonic Anhydrase. *J. Biol. Chem.* **246**, 2561–2573 (1971).
16. Mahon, B. P. *et al.* The structure of Carbonic Anhydrase IX is adapted for low-pH catalysis. *Biochemistry* **55**, 4642–4653 (2016).
17. Missner, A. *et al.* Carbon dioxide transport through membranes. *J. Biol. Chem.* **283**, 25340–25347 (2008).
18. Leem, C.-H. & Vaughan-Jones, R. D. Out-of-equilibrium pH transients in the guinea-pig ventricular myocyte. *J. Physiol.* **509**, 471–485 (1998).
19. Boyer, M. J. & Tannock, I. F. Regulation of intracellular pH in tumor cell lines: Influence of microenvironmental conditions. *Cancer Res.* **52**, 4441–4447 (1992).
20. Li, Y., Tu, C., Wang, H., Silverman, D. N. & Frost, S. C. Catalysis and pH control by membrane-associated carbonic anhydrase IX in MDA-MB-231 breast cancer cells. *J. Biol. Chem.* **286**, 15789–15796 (2011).
21. Hilvo, M. *et al.* Biochemical characterization of CA IX: One of the most active carbonic anhydrase isozymes. *J. Biol. Chem.* **283**, 27799–27809 (2008).
22. Wykoff, C. C. *et al.* Hypoxia-inducible expression of tumor associated carbonic anhydrases. *Cancer Res.* **60**, 7075–7083 (2000).
23. Song, C. W., Griffin, R. & Park, H. J. Influence of tumor pH on therapeutic response. In *Cancer Drug Resistance* (ed. Teicher, B. A.) 21–42 (Springer, Berlin, 2006).
24. Laget, S. *et al.* Technical insights into highly sensitiveisolation and molecular characterization of fixed and live circulating tumor cells for early detection of tumor invasion. *PLoS ONE* **12**, e0169427 (2017).
25. Kaelin, W. G. The von Hippel-Lindau tumor suppressor protein. *Annu. Rev. Cancer Biol.* **2**, 91–109 (2018).
26. Calzada, M. J. *et al.* von Hippel-Lindau tumor suppressor protein regulates the assembly of intercellular junctions in renal cancer cells through Hypoxia-Inducible Factor-independent mechanisms. *Cancer Res.* **66**, 1553–1560 (2006).
27. Karumanchi, A. S. *et al.* VHL tumor suppressor regulates Cl /HCO_3^- exchange and Na^+/H^+ exchange activities in renal carcinoma cells. *Physiol. Genomics* **5**, 119–128 (2001).
28. Leisz, S. *et al.* Distinct von Hippel-Lindau gene and hypoxia-regulated alterations in gene and protein expression patterns of renal cell carcinoma and their effects on metabolism. *Oncotarget* **6**, 11395–11406 (2015).
29. Puri, S., Cano, D. A. & Hebrok, M. A role for von Hippel-Lindau protein in pancreatic β-cell function. *Diabetes* **58**, 433–441 (2009).
30. Webb, S. D., Sherratt, J. A. & Fish, R. G. Mathematical modelling of tumour acidity: regulation of intracellular pH. *J. Theor. Biol.* **196**, 237–250 (1999).
31. Martin, N. K. *et al.* A mathematical model of tumour and blood pHe regulation: the HCO_3^-/CO_2 buffering system. *Math. Biosci.* **230**, 1–11 (2011).
32. Bouret, Y., Argentina, M. & Counillon, L. Capturing intracellular pH dynamics by coupling its molecular mechanisms within a fully tractable mathematical model. *PLoS ONE* **9**, e85449 (2014).
33. Hiremath, S. A. *et al.* Modeling of pH regulation in tumor cells: direct interaction between proton-coupled lactate transporters and cancer -associated carbonic anhydrase. *Math. Biosci. Eng.* **16**, 320–337 (2018).
34. Milotti, E., Vyshemirsky, V., Sega, M. & Chignola, R. Interplay between distribution of live cells and growth dynamics of solid tumours. *Sci. Rep.* **2**, 990 (2012).
35. Milotti, E., Vyshemirsky, V., Sega, M., Stella, S. & Chignola, R. Metabolic scaling in solid tumours. *Sci. Rep.* **3**, 1938 (2013).
36. Milotti, E., Stella, S. & Chignola, R. Pulsation-limited oxygen diffusion in the tumour microenvironment. *Sci. Rep.* **7**, 39762 (2017).
37. Fredrich, T., Rieger, H., Chignola, R. & Milotti, E. Fine-grained simulations of the microenvironment of vascularised tumours. *Sci. Rep.* **9**, 11698 (2019).
38. Helmlinger, G., Yuan, F., Dellian, M. & Jain, R. K. Interstitial pH and pO_2 gradients in solid tumors in vivo: high-resolution measurements reveal a lack of correlation. *Nat. Med.* **3**, 177–182 (1997).
39. McIntyre, A. *et al.* Disrupting hypoxia-induced bicarbonate transport acidifies tumor cells and suppresses tumor growth. *Cancer Res.* **76**, 3744–3755 (2016).
40. Mueller-Klieser, W. Method for the determination of oxygen consumption rates and diffusion coefficients in multicellular spheroids. *Biophys. J* . **46**, 343–348 (1984).
41. Deitmer, J. W. & Rose, C. R. pH regulation and proton signalling by glial cells. *Prog. Neurobiol.* **48**, 73–103 (1996).

42. Zhu, H. *et al.* Proton-sensing GPCR-YAP signalling promotes cell proliferation and survival. *Int. J. Biol. Sci.* **11**, 1181–1189 (2015).
43. Fredrich, T., Rieger, H., Chignola, R. & Milotti, E. Fine-grained simulations of the microenvironment of vascularized tumours. *Sci. Rep.* **9**, 11698 (2019).
44. Gibbons, B. H. & Edsall, J. T. Rate of hydration of carbon dioxide and dehydration of carbonic acid at 25. *J. Biol. Chem.* **238**, 3502–3507 (1963).
45. Sander, R. Compilation of Henry's law constants (version 4.0) for water as solvent. *Atmos. Chem. Phys.* **15**, 4399–4981 (2015).
46. Cassel, D., Katz, M. & Rotman, M. Depletion of cellular ATP inhibits Na^+/H^+ antiport in cultured human cells. Modulation of the regulatory effect of intracellular protons on the antiporter activity. *J. Biol. Chem.* **261**, 5460–5466 (1986).
47. Jandeleit-Dahm, K. *et al.* Diabetes-induced vascular hypertrophy is accompanied by activation of Na^+-H^+ exchange and prevented by Na^+-H^+ exchange inhibition. *Circ. Res.* **87**, 1133–1140 (2000).
48. Luo, J., Kintner, D. B., Shull, G. E. & Sun, D. ERK1/2-p90RSK-mediated phosphorylation of Na^+/H^+ exchanger isoform 1. A role in ischemic neuronal death. *J. Biol. Chem.* **282**, 28274–28284 (2007).
49. Alper, S. L. The band 3-related anion exchanger (AE) gene family. *Annu. Rev. Physiol.* **53**, 549–564 (1991).
50. Milotti, E., Del Fabbro, A. & Chignola, R. Numerical integration methods for large-scale biophysical simulations. *Comput. Phys. Commun.* **180**, 2166–2174 (2009).
51. Galassi, M. *et al. GNU Scientific Library* Vol. 3 (Network Theory Ltd, 2002).

Author contributions
R.C. and E.M. designed the research. R.C. found parameter values. N.P. and E.M. wrote C++ code. NP and RC carried out simulations. R.C. and E.M. wrote the article. All authors critically discussed results and revised the article.

Competing interests
The authors declare no competing interests.

Additional information
Supplementary information is available for this paper at https://doi.org/10.1038/s41598-020-70396-1.

Correspondence and requests for materials should be addressed to R.C.

Reprints and permissions information is available at www.nature.com/reprints.

Publisher's note Springer Nature remains neutral with regard to jurisdictional claims in published maps and institutional affiliations.

Open Access This article is licensed under a Creative Commons Attribution 4.0 International License, which permits use, sharing, adaptation, distribution and reproduction in any medium or format, as long as you give appropriate credit to the original author(s) and the source, provide a link to the Creative Commons license, and indicate if changes were made. The images or other third party material in this article are included in the article's Creative Commons license, unless indicated otherwise in a credit line to the material. If material is not included in the article's Creative Commons license and your intended use is not permitted by statutory regulation or exceeds the permitted use, you will need to obtain permission directly from the copyright holder. To view a copy of this license, visit http://creativecommons.org/licenses/by/4.0/.

© The Author(s) 2020

Supplementary Material

The control of acidity in tumor cells: a biophysical model

N. Piasentin [4][1], E. Milotti[2], and R. Chignola[3,*]

[1,2]Department of Physics, University of Trieste, Via Valerio 2, I-34127 Trieste, Italy
[3]Department of Biotechnology, University of Verona, Strada Le Grazie 15 - CV1, I-37134 Verona, Italy

In this document we detail the estimates of model parameters whenever not specified in the main text. In the Appendix we list the C++ code used for the simulations described in the Results section in the main text.

Rates of H^+ and CO_2 production

The rates of H^+ and CO_2 production are obtained from the metabolic model described in refs. (1, 2). To compute the rate of H^+ production by tumor cells we take into account the previously determined average rate of lactic acid production gAcL$\simeq 3.8 \cdot 10^{-19}$ kg s^{-1} (1). Under physiological conditions this acid completely dissociates to H^+ and lactate ions (2). Since these chemical species are in 1:1 molar ratio, the rate of H^+ production gH simply writes:

$$\mathrm{gH} = \mathrm{gAcL}\frac{\mathrm{MW_H}}{\mathrm{MW_{AcL}}}$$

where $\mathrm{MW_H} = 1$ g mol^{-1} and $\mathrm{MW_{AcL}} = 90$ g mol^{-1} are the molecular weights of H^+ and lactic acid.

Complete glucose oxidation requires 6 moles of O_2 per mole of glucose and in this reaction 6 moles of CO_2 are produced. Thus, if the respective rates of O_2 consumption and CO_2 production are qO_2 and gCO_2, we find:

$$\mathrm{gCO_2} = \mathrm{qO_2}\frac{\mathrm{MW_{CO_2}}}{\mathrm{MW_{O_2}}}$$

where $\mathrm{MW_{O_2}} = 32$ g mol^{-1} and $\mathrm{MW_{CO_2}} = 44$ g mol^{-1} are the molecular weights of O_2 and CO_2. Our previous work showed that for tumor cells on average $qO_2 \simeq 3.5 \cdot 10^{-20}$ kg s^{-1}.

Determination of parameters' values for NHE transporters

At least three independent experimental works confirmed that the activity of NHE transporters is described by a Hill equation (see also the main text) with exponent > 2 (3–5). In addition it has been reported that H^+ transport by NHE is inhibited by extracellular acidity (3).

To determine the values of parameters in equations that describe NHE transporters and their regulation by extracellular acidity we used the data in Fig.1, panel Ei, in ref. (3). The data have been obtained with careful measurements of H^+ fluxes in HCT116 cells (a human colorectal cancer cell line) with varying intracellular (pH_i) and extracellular (pH_e) pH. We redraw these data in figure S1.

We fitted these data with the following Hill equation:

$$\frac{dm_{\mathrm{H^+},C}}{dt} = \mathrm{V_{max}} \cdot \frac{[\mathrm{H^+}]_C^h}{K_\mathrm{m}^h + [\mathrm{H^+}]_C^h} \tag{1}$$

where square brackets denote molar concentrations, the subscript C is used for intracellular chemical species, $\mathrm{V_{max}}$ and K_m are the Michealis-Menten parameters and h is the Hill coefficient. Nonlinear fits were weighted with experimental errors and we used the χ^2/df statistics (df=degrees of freedom) to determine the goodness of the fits.

Best fit parameters values are listed in table S1. We take the average value of both K_m and h parameters calculated from the values shown in table S1, i.e. $K_\mathrm{m} = 0.1958 \pm 0.0124$ μM and $h = 2.67 \pm 0.15$, and the value of $\mathrm{V_{max}}$ estimated at $\mathrm{pH}_e = 7.4$. We compute the maximum ion flux per surface unit as $\mathrm{V_{max}}/\mathrm{S}_C$ where S_C is the cell surface. The reported radius of HCT116 cells is $\mathrm{r}_C = 6.55 \pm 0.14$ μm (3). We approximate the cell to a sphere and finally obtain the $\mathrm{V_{maxNHE}}$ value reported in Table 1 in the main text.

[4]current address: Department of Chemical and Process Engineering, University of Surrey, GU2 7XH, and Unilever R&D Colworth, Colworth Park, Sharnbook, Bedford MK44 1LQ, UK.

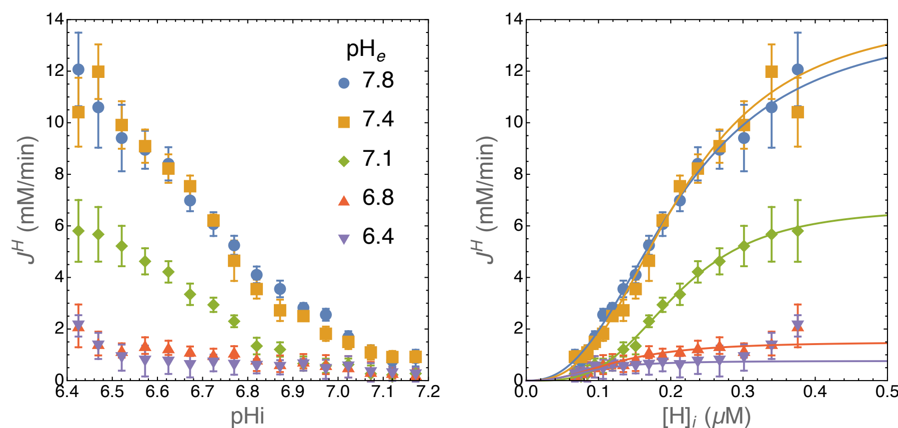

Figure S1: Fit of experimental data with equation 1. Left panel: the data taken in measurements of H^+ fluxes in HCT116 cells with varying pH_i and pH_e, redrawn from ref. (3). Right panel: same data as in the left panel, but in this case the x-axis has been converted from pH_i to intracellular H^+ concentration units. The lines show the best fits with the nonlinear Hill equation 1.

Table S1: Parameter values from nonlinear fits of the data in figure S1 with equation 1

pH_e	$V_{max}(mM/min)$	K_m (μM)	h	χ^2/df
7.8	13.99±2.18	0.2096±0.0277	2.47±0.25	1.22
7.4	14.31±1.70	0.2123±0.0199	2.71±0.22	1.24
7.1	6.73±1.18	0.2086±0.0242	3.44±0.53	1.20
6.8	1.51±0.46	0.1297±0.0438	2.43±1.30	1.24
6.4	0.76±0.42	0.0898±0.0473	2.68±3.81	1.32

To show how the V_{max} of NHE transporters varies with pH_e we plot the values listed in table S1 in figure S2. V_{max} values were divided by the maximum observed value (i.e. V_{max} estimated at pH_e=7.4) and then fitted with the following equation:

$$\text{fpHe} = \frac{1}{2}\left(1 + \frac{\text{pH}_\text{e} - \text{pH}_0}{\lambda + |\text{pH}_\text{e} - \text{pH}_0|}\right) \tag{2}$$

Equation 2 describe how extracellular pH affects the activity of NHE transporters by reducing the maximal rate of H^+ transport by the fraction fpH_e. Fit of the values in figure S2 with equation 2 yielded the following values for estimated parameters (χ^2/df = 1.85): $pH_{0,NHE} = 7.10 \pm 0.01$, $\lambda_{NHE} = 0.0759 \pm 0.0258$.

Determination of parameters' values for THCO3 transporters

We used the data in Fig.2 in (6) which show the dependence of proton fluxes in MGH U1 cells (a human bladder carcinoma cell line) on the extracellular concentration of bicarbonate ions. In these experiments the flux of protons is defined as the time variation of the product of pH_i and the buffering capacity of the cells (6). The data follow the Michaelis-Menten kinetics and thus:

$$\frac{dm_{\text{H}^+,C}}{dt} = \text{V}_{\text{max,H}} \cdot \frac{[\text{HCO}_3^-]_c}{K_\text{m} + [\text{HCO}_3^-]_c} \tag{3}$$

where, as usual, the square brackets denote molar concentrations and where the subscript C denotes the intracellular environment and c the extracellular one. Fitting the experimental data with equation 3 we find the following values for the Michaelis-Menten parameters (χ^2/df = 1.47, see figure S3): $V_{max,H} = 9.12 \pm 0.41$ mM/min, $K_m = 7.38 \pm 0.77$ mM. A fit of the same data with a Hill equation returned a value of 0.94 ± 0.09, i.e. $\simeq 1$, for the exponent, further indicating that the activity of bicarbonate transporters is not governed by Hill kinetics.

Equation 3 is rather unusual because it relates two different quantities, namely the molar concentrations of protons and of bicarbonate ions. Recalling that for a generic chemical species the molar concentration is related to mass by $[\text{X}] = m_\text{X}/(V \cdot \text{MW}_\text{X})$

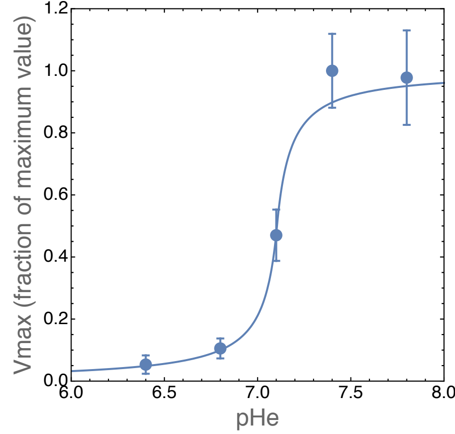

Figure S2: Plot of V_{max} values in table S1 (normalized with respect to the maximum reported value) as the function of extracellular pH. The line is the best fit with equation 2.

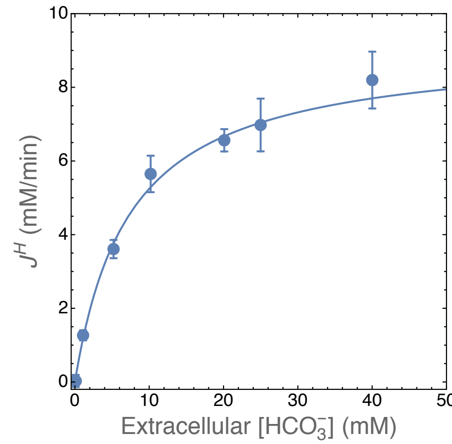

Figure S3: H^+ cell fluxes in MGH U1 cells as the function of extracellular concentration of HCO_3^- ions. Data have been redrawn from ref. (6). The line shows the best fit of experimental data with equation 3.

where V is the volume of the solution, then the left-hand side of equation 3 can be written as:

$$(\mathrm{MW_H} \cdot V_C) \times \frac{d[\mathrm{H}^+]_C}{dt} = \frac{dm_{\mathrm{H}^+,C}}{dt}$$

Thus:

$$\begin{aligned}
\frac{dm_{\mathrm{H}^+,C}}{dt} &= \mathrm{MW_H} \cdot V_C \cdot \mathrm{V_{max,H}} \cdot \frac{[\mathrm{HCO_3^-}]_c}{K_\mathrm{m} + [\mathrm{HCO_3^-}]_c} \\
&= \mathrm{MW_H} \cdot V_C \cdot \mathrm{V_{max,H}} \cdot \frac{m_{\mathrm{HCO_3^-},c}}{V_c \cdot \mathrm{MW_{HCO3}}} \cdot \frac{1}{K_\mathrm{m} + \frac{m_{\mathrm{HCO_3^-},c}}{V_c \cdot \mathrm{MW_{HCO3}}}} \\
&= \mathrm{MW_H} \cdot V_C \cdot \mathrm{V_{max,H}} \cdot \frac{m_{\mathrm{HCO_3^-},c}}{K_\mathrm{m} \cdot V_c \cdot \mathrm{MW_{HCO3}} + m_{\mathrm{HCO_3^-},c}}
\end{aligned}$$

Finally, to convert the H^+ mass into equivalent of HCO_3^- mass we multiply both sides by the molar mass ratio $\mathrm{MW_{HCO3}}/\mathrm{MW_H}$ and obtain:

$$\frac{dm_{HCO_3^-,c}}{dt} = \frac{\nu_{maxTHCO3} \cdot m_{HCO_3^-,c}}{K_{mTHCO3} \cdot V_c \cdot MW_{HCO3} + m_{HCO_3^-,c}}$$

where $\nu_{maxTHCO3} = MW_{HCO3} \cdot V_C \cdot V_{max,H}$ and $K_{mTHCO3} = K_m$. Using the previously estimated value of $V_{max,H}$, we find $\nu_{maxTHCO3} = 10.91 \cdot 10^{-3}$ pg s^{-1}. To obtain the maximum flux per surface unit we divide this value by the cell surface (we consider a cell radius $r_C = 6.55$ μm as in the previous section) so that, at the very end, $\nu_{maxTHCO3} = V_{maxTHCO3} \cdot S_C$ and $V_{maxTHCO3} = 2.024 \cdot 10^{-5}$ pg s^{-1} μm^{-2}.

It is known that the activity of bicarbonate transporters is regulated both by the intracellular and by the extracellular acidity (3, 7). To describe how bicarbonate fluxes depend upon pH_i we use the data in Fig.1, panel Biii, in ref. (7), while we use the data in Fig.2D in ref (3) to investigate how transport is affected by pH_e. The data were obtained by measuring proton fluxes in presence or in absence of the bicarbonate buffer. As explained in ref. (7), in the absence of the bicarbonate buffer only proton transporters are active, while in its presence both proton and bicarbonate transporters are active. The activity of THCO3 was then calculated by subtraction of these data.

As discussed in the main text we model this part with the following functions:

$$\mathrm{fpHi}_{THCO3} = \frac{1}{2}\{1 + \tanh[\gamma_{THCO3} \cdot (\mathrm{pHi}_{0,THCO3} - \mathrm{pH_i})]\} \tag{4}$$

$$\mathrm{fpHe}_{THCO3} = \frac{1}{2}\{1 + \tanh[\lambda_{THCO3} \cdot (\mathrm{pH_e} - \mathrm{pHe}_{0,THCO3})]\} \tag{5}$$

We fit these nonlinear equations to experimental data and the results are shown in figures S4. Since experimental errors were not reported along with the original data the goodness-of-fit statistics cannot be computed for these fits. The fits returned the following best values for the parameters: $\gamma_{THCO3} = 4.2 \pm 0.72$, $\mathrm{pHi}_{0,THCO3} = 6.9 \pm 0.02$, $\lambda_{THCO3} = 1.63 \pm 0.22$, $\mathrm{pHe}_{0,THCO3} = 6.85 \pm 0.04$.

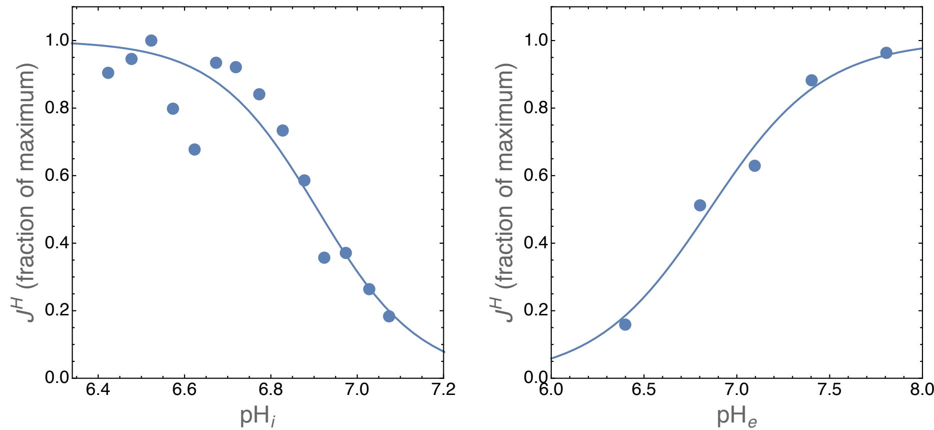

Figure S4: Activity of THCO3 transporters vs. extracellular and intracellular pH. Left panel: Symbols: data redrawn from ref. (7) and normalized with respect to the maximum observed value of J^H. Line: fit of experimental data with equation 4. Right panel: Symbols: data redrawn from ref. (3). The maximum flux J^H in this case was estimated by fit of raw data with a logistic equation. Line: fit of experimental data with equation 5.

The enzymatic activity of CA9

The enzyme CA9 follows the Michaelis-Menten kinetics. CA9 activity was measured by Li et al. (8) in experiments carried out with human breast cancer cells. They report the following values:

- initial CA9 concentration $[CA9]_0 = 1.3$ nM;
- kcat/Km = 62 ± 5 μM^{-1} s^{-1};

- reaction volume = 2 ml
- cell density = $5 \cdot 10^5$ cells/ml.

Using these values we calculated the Michaelis-Menten parameter $V_{max} = 0.58$ mM s^{-1} per cell. This value was then converted to CO_2 mass units and divided by the cell surface assuming a cell radius of 6.55 μm to obtain the value listed in Table 1 of the main text. The data in Tab.1 in ref. (9) show that the K_m of the CA9 kinetics varies between 6.9 to 7.5 mM when measured in different experimental conditions, and we choose to take the average value of $K_m = 7.2$ mM.

CA9 expression in cells depends on the environmental oxygen concentration. Wykoff et al. (10) measured its expression in A549 cells (a human lung carcinoma cell line) grown in normoxic (i.e. 20% O_2) or hypoxic environments by western-blot. We measured the density of the bands in western-blot experiments shown in Fig.3B of their paper (10) using the open-source image processing software ImageJ (version: 2.00-rc-69/1.52r) and the results are shown in figure S5.

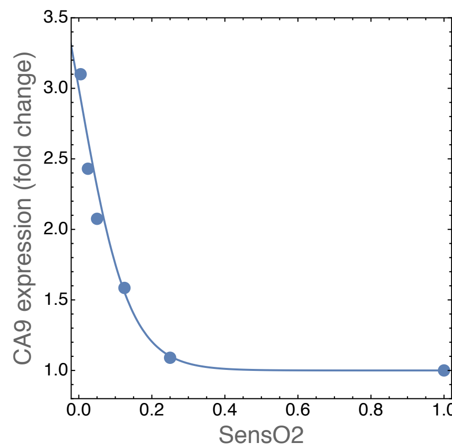

Figure S5: Expression of CA9 in cells grown under normoxic or hypoxic conditions. We used the software ImageJ to measure the density of the bands in western blots shown in Fig.3B in ref. (10). The results are expressed as fold-change expression with respect to CA9 protein band density observed for cells grown in a normoxic atmosphere (i.e. 20% O_2). The x-axis shows the fraction of oxygen to which the cells were exposed. This fraction corresponds to the parameter SensO2 in our model (see the main text). The data were fitted with equation 6 (line)

We fit the data with the following equation:

$$h_{CA9} = 3 + 2 \cdot \tanh\left(-\delta_{CA9} \cdot \mathrm{SensO2}\right) \tag{6}$$

and obtain $\delta_{CA9} \simeq 7.3$.

REFERENCES

1. Chignola, R., and E. Milotti, 2005. A phenomenological approach to the simulation of metabolism and proliferation dynamics of large tumour cell populations. *Physical Biology* 2:8–22.

2. Chignola, R., A. Delfabbro, C. Dalla Pellegrina, and E. Milotti, 2007. *Ab initio* phenomenological simulation of the growth of large tumor cell populations. *Physical Biology* 4:114–133.

3. Hulikova, A., R. D. Vaughan-Jones, and P. Swietach, 2011. Dual role of CO2/HCO3- buffer in the regulation of intracellular pH of three-dimensional tumor growths. *Journal of Biological Chemistry* 286:13815–13826.

4. Luo, J., D. B. Kintner, G. E. Shull, and D. Sun, 2007. ERK1/2-p90RSK-mediated phosphorylation of Na+/H+ exchanger isoform 1 A role in ischemic neuronal death. *Journal of Biological Chemistry* 282:28274–28284.

5. Jandeleit-Dahm, K., K. M. Hannan, C. A. Farrelly, T. J. Allen, J. R. Rumble, R. E. Gilbert, M. E. Cooper, and P. J. Little, 2000. Diabetes-induced vascular hypertrophy is accompanied by activation of Na+-H+ exchange and prevented by Na+-H+ exchange inhibition. *Circulation Research* 87:1133–1140.

6. Boyer, M. J., and I. F. Tannock, 1992. Regulation of intracellular pH in tumor cell lines: influence of microenvironmental conditions. *Cancer Research* 52:4441–4447.

7. Hulikova, A., A. L. Harris, R. D. Vaughan-Jones, and P. Swietach, 2013. Regulation of intracellular pH in cancer cell lines under normoxia and hypoxia. *Journal of Cellular Physiology* 228:743–752.

8. Li, Y., C. Tu, H. Wang, D. N. Silverman, and S. C. Frost, 2011. Catalysis and pH control by membrane-associated carbonic anhydrase IX in MDA-MB-231 breast cancer cells. *Journal of Biological Chemistry* 286:15789–15796.

9. Hilvo, M., L. Baranauskiene, A. M. Salzano, A. Scaloni, D. Matulis, A. Innocenti, A. Scozzafava, S. M. Monti, A. Di Fiore, G. De Simone, et al., 2008. Biochemical characterization of CA IX: one of the most active carbonic anhydrase isozymes. *Journal of Biological Chemistry* 283:27799–27809.

10. Wykoff, C. C., N. J. Beasley, P. H. Watson, K. J. Turner, J. Pastorek, A. Sibtain, G. D. Wilson, H. Turley, K. L. Talks, P. H. Maxwell, et al., 2000. Hypoxia-inducible expression of tumor associated carbonic anhydrases. *Cancer Research* 60:7075–7083.

Appendix: C++ code

We list the code used to carry out simulations.

```
1 // Author: Nicola Piasentin
2 // Master Thesis Project
3 // The control of acidity in tumour cells: a biophysical model
4 // GSL libraries needed
5
6 #include <iostream>
7 #include <iomanip>
8 #include <fstream>
9 #include <stdlib.h>
10 #include <math.h>
11 #include <stdio.h>
12 #include <gsl/gsl_vector.h>
13 #include <gsl/gsl_multiroots.h>
14
15 using namespace std;
16
17 ofstream outData, outDatapH;
18
19 double m_CO2_C_old, m_H_C_old, m_HCO3_C_old, m_CO2_c_old, m_H_c_old, m_HCO3_c_old;
20 const double Pi = M_PI;
21
22 // sensors
23 const double SensO2 = 1.0;
24 const double SensATP = 1.0;
25
26 struct cell_params
27 {
28   double MW_H;
29   double MW_CO2;
30   double MW_O2;
31   double MW_HCO3;
32   double MW_AcL;
33   double r_C;
34   double PM_CO2;
35   double gAcL;
36   double q_O2;
37   double k1;
38   double k2;
39   double VMAXAcL;
40   double K_mAcL;
41   double a2cH_slope;
42   double a2cH_thr;
43   double c2aH_slope;
44   double c2aH_thr;
45   double VMAXNHE;
```

```
46    double K_mNHE;
47    double a;
48    double l_NHE;
49    double pH0_NHE;
50    double VMAXTHCO3;
51    double K_mTHCO3;
52    double l_THCO3;
53    double pHe0_THCO3;
54    double g_THCO3;
55    double pHi0_THCO3;
56    double VMAXCA9;
57    double K_mCA9;
58    double d_CA9;
59    double V_c;
60    double dt;
61  };
62
63  int cell(const gsl_vector * x, void *params, gsl_vector * f)
64  {
65    double MW_H = ((struct cell_params *) params)->MW_H;
66    double MW_CO2 = ((struct cell_params *) params)->MW_CO2;
67    double MW_O2 = ((struct cell_params *) params)->MW_O2;
68    double MW_HCO3 = ((struct cell_params *) params)->MW_HCO3;
69    double MW_AcL = ((struct cell_params *) params)->MW_AcL;
70    double r_C = ((struct cell_params *) params)->r_C;
71    double PM_CO2 = ((struct cell_params *) params)->PM_CO2;
72    double gAcL = ((struct cell_params *) params)->gAcL;
73    double q_O2 = ((struct cell_params *) params)->q_O2;
74    double k1 = ((struct cell_params *) params)->k1;
75    double k2 = ((struct cell_params *) params)->k2;
76    double VMAXAcL = ((struct cell_params *) params)->VMAXAcL;
77    double K_mAcL = ((struct cell_params *) params)->K_mAcL;
78    double a2cH_slope = ((struct cell_params *) params)->a2cH_slope;
79    double a2cH_thr = ((struct cell_params *) params)->a2cH_thr;
80    double c2aH_slope = ((struct cell_params *) params)->c2aH_slope;
81    double c2aH_thr = ((struct cell_params *) params)->c2aH_thr;
82    double VMAXNHE = ((struct cell_params *) params)->VMAXNHE;
83    double K_mNHE = ((struct cell_params *) params)->K_mNHE;
84    double a = ((struct cell_params *) params)->a;
85    double l_NHE = ((struct cell_params *) params)->l_NHE;
86    double pH0_NHE = ((struct cell_params *) params)->pH0_NHE;
87    double VMAXTHCO3 = ((struct cell_params *) params)->VMAXTHCO3;
88    double K_mTHCO3 = ((struct cell_params *) params)->K_mTHCO3;
89    double l_THCO3 = ((struct cell_params *) params)->l_THCO3;
90    double pHe0_THCO3 = ((struct cell_params *) params)->pHe0_THCO3;
91    double g_THCO3 = ((struct cell_params *) params)->g_THCO3;
92    double pHi0_THCO3 = ((struct cell_params *) params)->pHi0_THCO3;
93    double VMAXCA9 = ((struct cell_params *) params)->VMAXCA9;
94    double K_mCA9 = ((struct cell_params *) params)->K_mCA9;
95    double d_CA9 = ((struct cell_params *) params)->d_CA9;
96    double V_c = ((struct cell_params *) params)->V_c;
97    double dt = ((struct cell_params *) params)->dt;
98
99    const double m_CO2_C = gsl_vector_get(x, 0);
100   const double m_H_C = gsl_vector_get(x, 1);
101   const double m_HCO3_C = gsl_vector_get(x, 2);
102   const double m_H_c = gsl_vector_get(x, 3);
103   const double m_HCO3_c = gsl_vector_get(x, 4);
104
105   // intracellular carbon dioxide dynamics
106   const double y0 = m_CO2_C - m_CO2_C_old - dt * (
107     // internal rate
108     SensO2 * q_O2 * MW_CO2 / MW_O2
109     // chemical equilibrium
110     - k1 * m_CO2_C + k2 * m_H_C * m_HCO3_C * 1000 * MW_CO2 / (4.0 / 3.0 * Pi * pow(r_C, 3.0) * MW_H *
      MW_HCO3)
111     // diffusion
112     + PM_CO2 * (m_CO2_c_old / V_c - m_CO2_C / (4.0 / 3.0 * Pi * pow(r_C, 3.0))) * (4.0 * Pi * pow(r_C,
      2.0))
```

```
113     );
114 
115   // intracellular hydrogen dynamics
116   const double y1 = m_H_C − m_H_C_old − dt ∗ (
117     // internal rate
118     SensATP ∗ gAcL ∗ MW_H / MW_AcL
119     // chemical equilibrium
120     + k1 ∗ m_CO2_C ∗ MW_H / MW_CO2 − k2 ∗ m_H_C ∗ m_HCO3_C ∗ 1000 / (4.0 / 3.0 ∗ Pi ∗ pow(r_C, 3.0) ∗
        MW_HCO3)
121     // nu_MCT_in−>out
122     − (2.0 − tanh(c2aH_slope ∗ (−log10(1000 ∗ m_H_C / (4.0 / 3.0 ∗ Pi ∗ pow(r_C, 3.0) ∗ MW_H))) −
        c2aH_thr)) ∗ VMAXAcL ∗ MW_H / MW_AcL
123     ∗ (4.0 ∗ Pi ∗ pow(r_C, 2.0)) ∗ m_H_C / ((4.0 / 3.0 ∗ Pi ∗ pow(r_C, 3.0)) ∗ K_mAcL ∗ MW_H / MW_AcL +
        m_H_C)
124     // nu_MCT_out−>in
125     + (2.0 − tanh(a2cH_slope ∗ (−log10(1000 ∗ m_H_c / (V_c ∗ MW_H))) − a2cH_thr)) ∗ VMAXAcL ∗ MW_H /
        MW_AcL
126     ∗ (4.0 ∗ Pi ∗ pow(r_C, 2.0)) ∗ m_H_c / (V_c ∗ K_mAcL ∗ MW_H / MW_AcL + m_H_c)
127     // nu _NHE_in−>out
128     − SensO2 ∗ SensATP ∗ 0.5 ∗ (1.0 + ((−log10(1000 ∗ m_H_c / (V_c ∗ MW_H))) − pH0_NHE) / (l_NHE + abs
        ((−log10(1000 ∗ m_H_c / (V_c ∗ MW_H))) − pH0_NHE)))
129     ∗ VMAXNHE ∗ (4.0 ∗ Pi ∗ pow(r_C, 2.0)) ∗ pow(m_H_C, a) / (pow(4.0 / 3.0 ∗ Pi ∗ pow(r_C, 3.0) ∗ MW_H
        ∗ K_mNHE / 1000, a) + pow(m_H_C, a))
130     );
131 
132   // intracellular bicarbonate ions dynamics
133   const double y2 = m_HCO3_C − m_HCO3_C_old − dt ∗ (
134     // chemical equilibrium
135     k1 ∗ MW_HCO3 / MW_CO2 ∗ m_CO2_C − k2 ∗ m_H_C ∗ m_HCO3_C ∗ 1000 / (4.0 / 3.0 ∗ Pi ∗ pow(r_C, 3.0) ∗
        MW_H)
136     // nu_THCO3_out−>in
137     + SensATP ∗ (0.5) ∗ (1.0 + tanh(l_THCO3 ∗ (−log10(1000 ∗ m_H_c / (V_c ∗ MW_H)) − pHe0_THCO3)))
138     ∗ (0.5) ∗ (1.0 + tanh(g_THCO3 ∗ (pHi0_THCO3 − (−log10(1000 ∗ m_H_C / (4.0 / 3.0 ∗ Pi ∗ pow(r_C,
        3.0) ∗ MW_H))))))
139     ∗ VMAXTHCO3 ∗ (4.0 ∗ Pi ∗ pow(r_C, 2.0)) ∗ m_HCO3_c / (V_c ∗ K_mTHCO3 ∗ MW_HCO3 / 1000 + m_HCO3_c)
140     );
141 
142   // extracellular hydrogen dynamics
143   const double y3 = m_H_c − m_H_c_old − dt ∗ (
144     // chemical equilibrium
145     k1 ∗ m_CO2_c_old ∗ MW_H / MW_CO2 − k2 ∗ m_H_c ∗ m_HCO3_c ∗ 1000 / (V_c ∗ MW_HCO3)
146     // nu_MCT_in−>out
147     + (2.0 − tanh(c2aH_slope ∗ (−log10(1000 ∗ m_H_C / (4.0 / 3.0 ∗ Pi ∗ pow(r_C, 3.0) ∗ MW_H))) −
        c2aH_thr)) ∗ VMAXAcL ∗ MW_H / MW_AcL
148     ∗ (4.0 ∗ Pi ∗ pow(r_C, 2.0)) ∗ m_H_C / ((4.0 / 3.0 ∗ Pi ∗ pow(r_C, 3.0)) ∗ K_mAcL ∗ MW_H / MW_AcL +
        m_H_C)
149     // nu_MCT_out−>in
150     − (2.0 − tanh(a2cH_slope ∗ (−log10(1000 ∗ m_H_c / (V_c ∗ MW_H))) − a2cH_thr)) ∗ VMAXAcL ∗ MW_H /
        MW_AcL
151     ∗ (4.0 ∗ Pi ∗ pow(r_C, 2.0)) ∗ m_H_c / (V_c ∗ K_mAcL ∗ MW_H / MW_AcL + m_H_c)
152     // nu _NHE_in−>out
153     + SensATP ∗ SensO2 ∗ 0.5 ∗ (1.0 + ((−log10(1000 ∗ m_H_c / (V_c ∗ MW_H))) − pH0_NHE) / (l_NHE + abs
        ((−log10(1000 ∗ m_H_c / (V_c ∗ MW_H))) − pH0_NHE)))
154     ∗ VMAXNHE ∗ (4.0 ∗ Pi ∗ pow(r_C, 2.0)) ∗ pow(m_H_C, a) / (pow(4.0 / 3.0 ∗ Pi ∗ pow(r_C, 3.0) ∗ MW_H
        ∗ K_mNHE / 1000, a) + pow(m_H_C, a))
155     // nu_CA9
156     + (3.0 + 2.0 ∗ tanh(−d_CA9 ∗ SensO2)) ∗ VMAXCA9 ∗ 4.0 ∗ Pi ∗ pow(r_C, 2.0) ∗ m_CO2_c_old / (V_c ∗
        K_mCA9 ∗ MW_CO2 / 1000 + m_CO2_c_old)
157     ∗ MW_H / MW_CO2
158     );
159 
160   // extracellular bicarbonate ions dynamics
161   const double y4 = m_HCO3_c − m_HCO3_c_old − dt ∗ (
162     // chemical equilibrium
163     k1 ∗ m_CO2_c_old ∗ MW_HCO3 / MW_CO2 − k2 ∗ m_H_c ∗ m_HCO3_c ∗ 1000 / (V_c ∗ MW_H)
164     // nu_THCO3_out−>in
165     − SensATP ∗ (0.5) ∗ (1.0 + tanh(l_THCO3 ∗ (−log10(1000 ∗ m_H_c / (V_c ∗ MW_H)) − pHe0_THCO3)))
166     ∗ (0.5) ∗ (1.0 + tanh(g_THCO3 ∗ (pHi0_THCO3 − (−log10(1000 ∗ m_H_C / (4.0 / 3.0 ∗ Pi ∗ pow(r_C,
        3.0) ∗ MW_H))))))
```

```
167     * VMAXTHCO3 * (4.0 * Pi * pow(r_C, 2.0)) * m_HCO3_c / (V_c * K_mTHCO3 * MW_HCO3 / 1000 + m_HCO3_c)
168     // nu_CA9
169     + (3.0 + 2.0 * tanh(-d_CA9 * SensO2)) * VMAXCA9 * 4.0 * Pi * pow(r_C, 2.0) * m_CO2_c_old / (V_c *
        K_mCA9 * MW_CO2 / 1000 + m_CO2_c_old)
170     * MW_HCO3 / MW_CO2
171     );
172
173   gsl_vector_set(f, 0, y0);
174   gsl_vector_set(f, 1, y1);
175   gsl_vector_set(f, 2, y2);
176   gsl_vector_set(f, 3, y3);
177   gsl_vector_set(f, 4, y4);
178
179   return GSL_SUCCESS;
180 }
181
182 int main(void)
183 {
184   const gsl_multiroot_fsolver_type *T;
185   gsl_multiroot_fsolver *s;
186
187   int status, time, j, k, perc;
188   double dt, pH;// , pH_temp;
189   size_t iter = 0;
190
191   // respect units!
192   const double MW_H = 1.0; // g/mol
193   const double MW_CO2 = 44.0; // g/mol
194   const double MW_O2 = 32.0; // g/mol
195   const double MW_HCO3 = 61.0; // g/mol
196   const double MW_AcL = 90.1; // g/mol
197   const double r_C = 6.55; // mim
198   const double PM_CO2 = 3.2 * pow(10, 4); // mim/s
199   const double gAcL = 3.8 * pow(10, -4); // pg/s
200   const double q_O2 = 3.5 * pow(10, -5); // pg/s
201   const double k1 = 0.144; // 1/s
202   const double k2 = 1.9 * pow(10, 5); // 1/(M*s)
203   const double VMAXAcL = 9.58 * pow(10, -5); // pg/(s*mim^2)
204   const double K_mAcL = 0.405 * pow(10, -3); // pg/mim^3
205   const double a2cH_slope = 1.5; // adim
206   const double a2cH_thr = 7.0; // adim
207   const double c2aH_slope = 1.5; // adim
208   const double c2aH_thr = 7.0; // adim
209   const double VMAXNHE = 5.15 * pow(10, -7); // pg/(s*mim^2)
210   const double K_mNHE = 0.196 * pow(10, -6); // pg/mim^3
211   const double a = 2.67; // adim
212   const double l_NHE = 0.076; // adim
213   const double pH0_NHE = 7.1; // adim
214   const double VMAXTHCO3 = 2.02 * pow(10, -5); // pg/(s*mim^2)
215   const double K_mTHCO3 = 7.38 * pow(10, -3); // pg/mim^3
216   const double l_THCO3 = 1.63; // adim
217   const double pHe0_THCO3 = 6.85; // adim
218   const double g_THCO3 = 4.2; // adim
219   const double pHi0_THCO3 = 6.90; // adim
220   const double VMAXCA9 = 9.47 * pow(10, -2); // pg/(s*mim^2)
221   const double K_mCA9 = 7.2 * pow(10, -3); // pg/mim^3
222   const double d_CA9 = 7.3; // adim
223   const double V_c = 1.0 * pow(10, 12); // mim^3
224   const double pKa = -log10(k1 / k2); // adim
225   const double pH_cell = 7.40;  // adim
226
227   const int max_iter = 1000; // max number of iterations for Newton-Raphson
228
229   // input from the user
230   cout << "Time interval: " << endl;
231   cin >> dt;
232   cout << "Total integration time: " << endl;
233   cin >> time;
234   cout << "Starting pH: " << endl;
```

```
cin >> pH;

// starting conditions
m_CO2_C_old = 5.39 * pow(10.0, -5) * (4.0 / 3.0 * Pi * pow(r_C, 3.0));
m_H_C_old = pow(10.0, -pH_cell - 3.0) * (4.0 / 3.0 * Pi * pow(r_C, 3.0));
m_HCO3_C_old = MW_HCO3 / MW_CO2 * m_CO2_C_old * pow(10.0, pH_cell - pKa);

m_CO2_c_old = 5.39 * pow(10.0, -5) * V_c;
m_H_c_old = pow(10.0, -pH - 3.0) * V_c;
m_HCO3_c_old = MW_HCO3 / MW_CO2 * m_CO2_c_old * pow(10.0, pH - pKa);

// friendly reminder
cout << endl;
cout << "**********************************************" << endl;
cout << endl;
cout << "Starting parameters" << endl;
cout << endl;
cout << "m_CO2_C  (pg): " << m_CO2_C_old << endl;
cout << "m_H_C    (pg): " << m_H_C_old << endl;
cout << "m_HCO3_C (pg): " << m_HCO3_C_old << endl;
cout << "m_CO2_c  (pg): " << m_CO2_c_old << endl;
cout << "m_H_c    (pg): " << m_H_c_old << endl;
cout << "m_HCO3_c (pg): " << m_HCO3_c_old << endl;
cout << "V_c   (mim^3): " << V_c << endl;
cout << "dt:            " << dt << endl;
cout << "steps:         " << time << endl;
cout << "time:          " << time * dt << endl;
cout << "starting pH:   " << pH << endl;
cout << "sensO2:        " << SensO2 << endl;
cout << "sensATP:       " << SensATP << endl;
cout << endl;
cout << "**********************************************" << endl;
cout << endl;
cout << "Running..." << endl;
cout << endl;

// FYI
perc = 10;
cout << "-- completed at: 0 %" << endl;

const size_t n = 5;
struct cell_params cell_p = { MW_H, MW_CO2, MW_O2, MW_HCO3, MW_AcL, r_C, PM_CO2, gAcL, q_O2, k1, k2, VMAXAcL, K_mAcL, a2cH_slope,
  a2cH_thr, c2aH_slope, c2aH_thr, VMAXNHE, K_mNHE, a, l_NHE, pH0_NHE, VMAXTHCO3, K_mTHCO3, l_THCO3,
  pHe0_THCO3, g_THCO3, pHi0_THCO3, VMAXCA9, K_mCA9, d_CA9, V_c, dt };

gsl_multiroot_function cell_f = { &cell, n, &cell_p };

double x_init[n] = { m_CO2_C_old, m_H_C_old, m_HCO3_C_old, m_H_c_old, m_HCO3_c_old }; // starting point
gsl_vector *x = gsl_vector_alloc(n);

for (k = 0; k < n; k++)
{
  gsl_vector_set(x, k, x_init[k]);
}

T = gsl_multiroot_fsolver_dnewton; // discrete Newton (discrete Jacobian)
s = gsl_multiroot_fsolver_alloc(T, n);

gsl_multiroot_function f = cell_f;

outData.open("cell_output.txt"); // output masses
outDatapH.open("cell_output_pH.txt"); // output pH

gsl_multiroot_fsolver_set(s, &f, x);

// output on masses file
outData << "# Starting parameters" << endl;
```

```
302   outData << endl;
303   outData << "# m_CO2_C   (pg): " << m_CO2_C_old << endl;
304   outData << "# m_H_C     (pg): " << m_H_C_old << endl;
305   outData << "# m_HCO3_C (pg): " << m_HCO3_C_old << endl;
306   outData << "# m_CO2_c   (pg): " << m_CO2_c_old << endl;
307   outData << "# m_H_c     (pg): " << m_H_c_old << endl;
308   outData << "# m_HCO3_c (pg): " << m_HCO3_c_old << endl;
309   outData << "# V_c    (mim^3): " << V_c << endl;
310   outData << "# dt:             " << dt << endl;
311   outData << "# steps:          " << time << endl;
312   outData << "# time:           " << time * dt << endl;
313   outData << "# starting pH:    " << pH << endl;
314   outData << "# sensO2:         " << SensO2 << endl;
315   outData << "# sensATP:        " << SensATP << endl;
316   outData << endl;
317   outData << "# step\tm_CO2_C\tm_H_C\tm_HCO3_C\tm_H_c\tm_HCO3_c" << endl;
318   outData << endl;
319
320   // output on pH file
321   outDatapH << "# Starting parameters" << endl;
322   outDatapH << endl;
323   outDatapH << "# m_CO2_C   (pg): " << m_CO2_C_old << endl;
324   outDatapH << "# m_H_C     (pg): " << m_H_C_old << endl;
325   outDatapH << "# m_HCO3_C (pg): " << m_HCO3_C_old << endl;
326   outDatapH << "# m_CO2_c   (pg): " << m_CO2_c_old << endl;
327   outDatapH << "# m_H_c     (pg): " << m_H_c_old << endl;
328   outDatapH << "# m_HCO3_c (pg): " << m_HCO3_c_old << endl;
329   outDatapH << "# V_c    (mim^3): " << V_c << endl;
330   outDatapH << "# dt:             " << dt << endl;
331   outDatapH << "# steps:          " << time << endl;
332   outDatapH << "# time:           " << time * dt << endl;
333   outDatapH << "# starting pH:    " << pH << endl;
334   outDatapH << "# sensO2:         " << SensO2 << endl;
335   outDatapH << "# sensATP:        " << SensATP << endl;
336   outDatapH << endl;
337   outDatapH << "# step\tpH_C\tpH_c\tpH_C HH\tpH_c HH" << endl;
338   outDatapH << endl;
339
340   // gonna need them
341   outData << fixed;
342   outData << setprecision(15);
343
344   outDatapH << fixed;
345   outDatapH << setprecision(15);
346
347   // first term
348   outData << "0" << "\t" << m_CO2_C_old << "\t" << m_H_C_old << "\t" << m_HCO3_C_old << "\t" <<
        m_H_c_old << "\t" << m_HCO3_c_old << endl;
349   outDatapH << "0" << "\t"
350     << -log10(1000 * m_H_C_old / (4.0 / 3.0 * Pi * pow(r_C, 3.0))) << "\t"
351     << -log10(1000 * m_H_c_old / V_c) << "\t" << log10((m_HCO3_C_old * MW_CO2 * k2) / (m_CO2_C_old *
        MW_HCO3 * k1))
352     << "\t" << log10((m_HCO3_c_old * MW_CO2 * k2) / (m_CO2_c_old * MW_HCO3 * k1)) << endl;
353
354   // starts the time
355   for (j = 1; j < time; j++)
356   {
357     iter = 0;
358
359     do
360     {
361       iter++;
362
363       status = gsl_multiroot_fsolver_iterate(s);
364
365       if (status)   // check if solver is stuck
366         break;
367
368       status = gsl_multiroot_test_residual(s->f, 1e-6);
```

```
369
370     } while (status == GSL_CONTINUE && iter < max_iter);
371
372     // lazy...
373     if (j * 100 / time == perc)
374     {
375       cout << "-- completed at: " << perc << " %" << endl;
376       perc = perc + 10;
377     }
378
379     // output control
380     if (j % 100 == 0)
381     {
382
383       outData << j * dt << "\t" << gsl_vector_get(s->x, 0) << "\t" << gsl_vector_get(s->x, 1) << "\t"
    << gsl_vector_get(s->x, 2)
384         << "\t" << gsl_vector_get(s->x, 3) << "\t" << gsl_vector_get(s->x, 4) << endl;
385
386       outDatapH << j * dt << "\t"
387         << -log10(1000 * gsl_vector_get(s->x, 1) / (4.0 / 3.0 * Pi * pow(r_C, 3.0))) << "\t"
388         << -log10(1000 * gsl_vector_get(s->x, 3) / V_c)
389         << "\t" << log10((gsl_vector_get(s->x, 2) * MW_CO2 * k2) / (gsl_vector_get(s->x, 0) * MW_HCO3 *
   k1))
390         << "\t" << log10((gsl_vector_get(s->x, 4) * MW_CO2 * k2) / (m_CO2_c_old * MW_HCO3 * k1)) <<
    endl;
391
392     }
393
394     x_init[0] = gsl_vector_get(s->x, 0);
395     x_init[1] = gsl_vector_get(s->x, 1);
396     x_init[2] = gsl_vector_get(s->x, 2);
397     x_init[3] = gsl_vector_get(s->x, 3);
398     x_init[4] = gsl_vector_get(s->x, 4);
399
400     m_CO2_C_old = x_init[0];
401     m_H_C_old = x_init[1];
402     m_HCO3_C_old = x_init[2];
403     m_H_c_old = x_init[3];
404     m_HCO3_c_old = x_init[4];
405
406     // pH drop at time j*dt
407     /*
408     if (j == 200000)
409     {
410       m_H_C_old = m_H_C_old * pow(10.0, 1.0);
411       pH_temp = -log10(m_H_C_old * 1000.0 / (4.0 / 3.0 * Pi * pow(r_C, 3.0) * MW_H));
412       m_HCO3_C_old = MW_HCO3 / MW_CO2 * m_CO2_C_old * pow(10.0, pH_temp - pKa);
413       x_init[1] = m_H_C_old;
414       x_init[2] = m_HCO3_C_old;
415     }
416     */
417
418     for (k = 0; k < n; k++)
419     {
420       gsl_vector_set(x, k, x_init[k]);
421     }
422
423     gsl_multiroot_fsolver_set(s, &f, x);
424
425   }
426
427   // closing
428   cout << "-- completed at: " << perc << " %" << endl;
429   cout << "-- done!" << endl;
430   cout << endl;
431
432   gsl_multiroot_fsolver_free(s);
433   gsl_vector_free(x);
434
```

```
435    outData.close();
436    outDatapH.close();
437
438    // because windows
439    system("pause");
440
441    return 0;
442
443 }
```